

ABSTRACT

Title of Thesis: A STATISTICAL STUDY OF MIXED WAVE SYSTEMS

Ke Ma, Master of Science, 2018

Thesis Directed By: Professor Thomas Antonsen,
Department of Electrical and Computer
Engineering

Mixed wave systems are systems governed by wave equations that in the semiclassical limit have coexisting chaotic and regular trajectories. The goal of this study is to calculate the statistics of the response of mixed systems to external excitation. The ray tracing method is used to explore the property of simple two-dimensional wave system shapes: the “Four Arcs” and the “Peanut” billiard. The ray trajectories for these two mixed systems are plotted in real space and in phase space. The goal is to apply the generalized Random Coupling Model (RCM) to study the response of these two mixed systems in the form of their impedance matrices. To obtain information needed for the generalized RCM, the Method of Moments (MOM) is implemented to numerically calculate the eigenfrequencies and eigenmodes of the 2D cavities under consideration. As a preliminary study statistics of a lossless and a lossy impedance for a two-port 2D rectangular cavity are calculated.

A STATISTICAL STUDY OF MIXED WAVE SYSTEMS

by

Ke Ma

Thesis submitted to the Faculty of the Graduate School of the
University of Maryland, College Park, in partial fulfillment
of the requirements for the degree of
Master of Science
2018

Advisory Committee:
Professor Thomas Antonsen, Chair
Professor Edward Ott
Professor Steven Anlage

© Copyright by
Ke Ma
2018

Acknowledgements

First, I would like to thank my advisor Prof. Antonsen for guiding me through my M.S. study. It is my great honor to work with him from August 2015 to May 2018. He gives me many good suggestions. I have learnt a lot from Prof. Antonsen's rich experience in computational electromagnetics and numerical analysis. Also I would like to thank my co-advisors, Prof. Ott and Prof. Anlage, for their guidance to my M.S. study.

Second, I want to thank the fellow students in my wave chaos research group: Trystan Koch, Bisrat Addissie, Farasatul Adnan, Bo Xiao, Ziyuan Fu, and Min Zhou for their assistance and discussions. I also appreciate the help from my Electrical Engineering Department administrative staffs, especially graduate program director Melanie Prange, Bill Churma, and Heather Stewart.

Thanks to Prof. Loris Magnani for caring about me.

At last, I would like to thank my parents for their unconditional love, support and encouragement.

Table of Contents

Acknowledgements.....	ii
Table of Contents.....	iii
List of Abbreviations.....	v
Chapter 1: Introduction.....	1
1.1 Motivation.....	1
1.2 Wave Chaos.....	2
1.2.1 Weyl’s Formula and Normalized Spacing.....	2
1.2.2 Random Matrix Theory.....	3
1.2.3 Random Plane Wave Hypothesis.....	5
1.3 The RCM and the Generalized RCM on Cavity Impedance.....	6
1.3.1 Regular, Chaotic and Mixed System Cavities.....	6
1.3.2 The RCM on Chaotic System Cavity Impedance.....	7
1.3.3 The Generalized RCM on Mixed System Cavity Impedance.....	9
1.4 Outline of Thesis.....	10
Chapter 2: Mixed System Billiard.....	12
2.1 Four Arcs Billiard.....	12
2.1.1 Setup.....	12
2.1.2 Four Arcs Billiard Trajectories in Real Space and in Phase Space.....	14
2.2 Peanut Billiard.....	18
2.2.1 Setup.....	18
2.2.2 Peanut Billiard Trajectories in Real Space and in Phase Space.....	19
Chapter 3: The Method of Moments on Eigenfrequencies and Eigenmodes of 2D Cavities.....	23
3.1 Method of Moments in 2D Cavity Problems.....	24
3.1.1 Transform Homogenous Helmholtz Equation into Matrix Equation.....	24
3.1.2 Evaluate the Coefficient Matrix of the Helmholtz Matrix Equation.....	27
3.1.3 Solve the Homogenous Helmholtz Equation Numerically.....	29
3.2 Implement the Method of Moments on the Circular, the Four Arcs and the Peanut Cavities.....	30
3.2.1 Eigenfrequencies and Eigenmodes of the Circular Cavity.....	30
3.2.2 Eigenfrequencies and Eigenmodes of the Four Arcs Cavity.....	33
3.2.3 Eigenfrequencies and Eigenmodes of the Peanut Cavity.....	36
Chapter 4: Statistical Study of a Two-Port 2D Rectangular Cavity Impedance.....	39
4.1 Setup.....	39
4.2 Impedance for Lossless Two-Port 2D Rectangular Cavity.....	40
4.2.1 Formulas for Lossless Impedance.....	40
4.2.2 Lossless Dimensionless Reactance PDF Using Numerical Eigenmodes vs. Using the RCM.....	44
4.3 Impedance for Lossy Two-Port 2D Rectangular Cavity.....	46
4.3.1 Formulas for Lossy Impedance.....	46
4.3.2 Lossy Dimensionless Impedance PDF Using Numerical Eigenmodes vs. Using the RCM.....	48

Chapter 5: Summary and Future Work.....	52
5.1 Summary.....	52
5.2 Future Work.....	52
Bibliography.....	54

List of Abbreviations

RCM	Random Coupling Model
MOM	Method of Moments
GOE	Gaussian orthogonal ensemble
PDF	probability density function
Q	cavity quality factor
A	enclosed area of 2D cavity
ϕ_n	the eigenfunction of the nth eigenmode
k	wave number
$\Delta(k^2)$	adjacent eigenvalues mean spacing
\mathbf{Z}	impedance matrix
ζ	dimensionless impedance matrix
\mathbf{E}	dimensionless reactance matrix
ρ	dimensionless resistance matrix

Chapter 1: Introduction

1.1 Motivation

Calculating the electromagnetic response of enclosures is a general and challenging problem in electromagnetics and microwave engineering. For a given configuration of an enclosure, technically the electromagnetic response can be solved through the deterministic approach. That is, solve the governing electromagnetic equations with boundary conditions and obtain the electromagnetic quantities numerically. However, this deterministic approach is not always feasible if we take the cost of computation time and computational resources into account, and we allow for uncertainty in the exact dimensions and contents of the enclosure. That is especially true when you have a very complicated shaped enclosure.

What makes the problem complicated is that, when the wavelength is very small compared with the size of the enclosure, the electromagnetic quantities are highly sensitive to small enclosure configuration changes. Therefore in the deterministic approach you have to solve the same electromagnetic equations repeatedly for slightly different configurations. Likewise the deterministic approach also has drawback with small changes in frequency: since in practice a microwave system is very often operating in a wide frequency range. Consequently you must solve the same electromagnetic equations once per each frequency of interest.

The deterministic approach's drawback motivates people to employ a statistical approach to solve the electromagnetic quantities, or at least to characterize them

probabilistically. This kind of statistical approach was first introduced by Wigner in his study of the energy levels of large nuclei [1-3].

In my thesis, I focus on quasi-2D cavities with ports. And the electromagnetic quantity I'm trying to determine is the cavity impedance. I will characterize the cavity impedance through the statistical approach based on the Random Coupling Model (RCM) [1-3].

1.2 Wave Chaos

Here I introduce concepts relevant to the understanding of wave properties for complicated enclosure [1-3].

1.2.1 Weyl's Formula and Normalized Spacing

Solution of the wave equation in a 2D domain with Dirichlet and Neumann boundary condition is an eigenvalue problem for which there is a discrete set of eigenfunctions and corresponding eigenvalues k_n^2 , $n = 1, 2, \dots$. Here has of wave number and $\lambda = 2\pi/k_n$ is the free space wavelength of the waves form the eigenfunction.

For my 2D problem, in an enclosed region Ω of area A , the number of eigenmodes below k^2 (i.e. $k_n^2 < k^2$) is given by Weyl's formula [1-3]:

$$N(k^2) = \frac{A}{4\pi} k^2 + O(k), \quad (1.1)$$

From Eq. (1.1), we can write the average mode density of a 2D enclosure approximately as:

$$\rho(k^2) \approx \frac{A}{4\pi}, \quad (1.2)$$

Therefore, the mean spacing between adjacent eigenvalues ($\Delta(k^2) \equiv \langle k_{n+1}^2 - k_n^2 \rangle$) is:

$$\Delta(k^2) = \frac{1}{\rho(k^2)} = \frac{4\pi}{A}, \quad (1.3)$$

We define the normalized eigenvalue spacing as:

$$s_n = \frac{k_{n+1}^2 - k_n^2}{\Delta(k^2)} = \tilde{k}_{n+1}^2 - \tilde{k}_n^2, \quad (1.4)$$

The probability density function (PDF) of s_n has been well studied for wave systems, and it will be used in Random Coupling Model (RCM) later on.

1.2.2 Random Matrix Theory

When studying the energy spectra of large nuclei, Wigner found the wave equation was difficult to solve, so instead he characterize the energy spectra by statistics. Winger's hypothesis is that the eigenvalue spectra of heavy nuclei have similar statistical properties to the spectra of some carefully designed random matrices. Depending on different types of symmetry, Winger designed three kinds of random matrix ensembles, they are [1, 3, 4]: Gaussian Orthogonal Ensemble (GOE), Gaussian Unitary Ensemble (GUE) and Gaussian Symplectic Ensemble (GSE). In my thesis I only employ the GOE. And a GOE random matrix \mathbf{H} should have these two properties:

1. *Invariance.* The probability distribution for the elements of \mathbf{H} , $\bar{P}(\mathbf{H})$, should be invariant to orthogonal transformations of \mathbf{H} :

$$\bar{P}(\mathbf{H}) = \bar{P}(\mathbf{O}\mathbf{H}\mathbf{O}^T), \quad (1.5)$$

where \mathbf{O} denotes any orthogonal matrix.

2. *Independence.* The GOE matrix elements are independent random variables.

The probability distribution $\bar{P}(\mathbf{H})$ is the product of distributions for the individual elements $H_{ij}, i \leq j$.

Based on the above two properties, we generate a GOE random matrix \mathbf{H} as followed:

$$\begin{aligned} H_{ij} &\sim N(0,1), \text{ when } i = j, \\ H_{ij} &\sim N(0,1/2), \text{ when } i < j, \\ H_{ij} &= H_{ji}, \end{aligned} \tag{1.6}$$

where $N(\mu, \sigma^2)$ denotes a Gaussian distribution random variable with mean μ and variance σ^2 .

For GOE random matrices, Wigner found that the normalized eigenvalue spacing obeys this probability distribution function [1, 2]:

$$P_{GOE}(s) \approx \frac{\pi}{2} s \text{Exp} \left(-\frac{\pi}{4} s^2 \right), \tag{1.7}$$

In contrast, the normalized eigenvalue spacing of a regular system (system which only has regular ray trajectories) obeys Poisson distribution:

$$P_{Poisson}(s) = e^{-s}, \tag{1.8}$$

As an example, I generate a 5000×5000 GOE random matrix according to Eq. (1.6), and plot its normalized eigenvalue spacing s_n (according to Eq. (1.4)) probability distribution function (PDF) histogram in Fig. 1.1, along with the theoretical PDF predictions of Eq. (1.7) and (1.8).

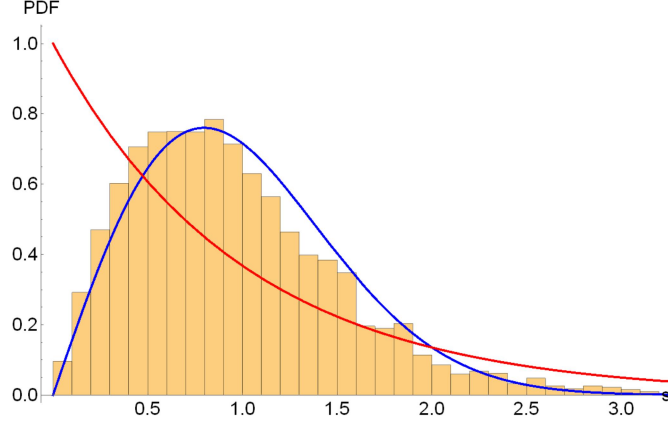


Figure 1.1: Normalized eigenvalue spacing probability distribution function (PDF) histogram of a 5000×5000 GOE random matrix (yellow histogram) vs. theoretical PDF predictions of $P_{GOE}(s)$ Eq. (1.7) (blue line) and $P_{Poisson}(s)$ Eq. (1.8) (red line).

1.2.3 Random Plane Wave Hypothesis

The Berry's random plane wave hypothesis says: At short wavelength, at a randomly chosen position \vec{x} inside a pure chaotic system Ω , the wave function evaluated at this position $\phi_n(\vec{x})$ has statistical properties similar to a random, isotropic superposition of many plane waves [2, 3].

$$\phi_n(\vec{x}) \approx \text{Re} \left[\sum_{j=1}^N \alpha_j \text{Exp}(ik_n \vec{e}_j \cdot \vec{x} + i\beta_j) \right], \quad N \gg 1, \quad (1.9)$$

where the wave number k_n is fixed, but the amplitudes α_j , propagation direction \vec{e}_j , and phases β_j are random variables.

Based on this random plane wave hypothesis, we can replace $\phi_n(\vec{x})$ by a Gaussian random variable. For a 2D enclosure Ω of enclosed area A , the PDF of $\phi_n(\vec{x})$ is given as:

$$P(\phi_n) = \frac{1}{\sqrt{2\pi\sigma^2}} \text{Exp}\left[-\frac{\phi_n^2}{2\sigma^2}\right], \quad \text{where variance } \sigma^2 = 1/A, \quad (1.10)$$

1.3 The RCM and the Generalized RCM on Cavity Impedance

1.3.1 Regular, Chaotic and Mixed System Cavities

To explain the concept of regular, chaotic and mixed systems, we first need to explain what regular and chaotic ray trajectories are. Fig. 1.2 is an illustration of regular and chaotic ray trajectories in the Mushroom cavity [3].

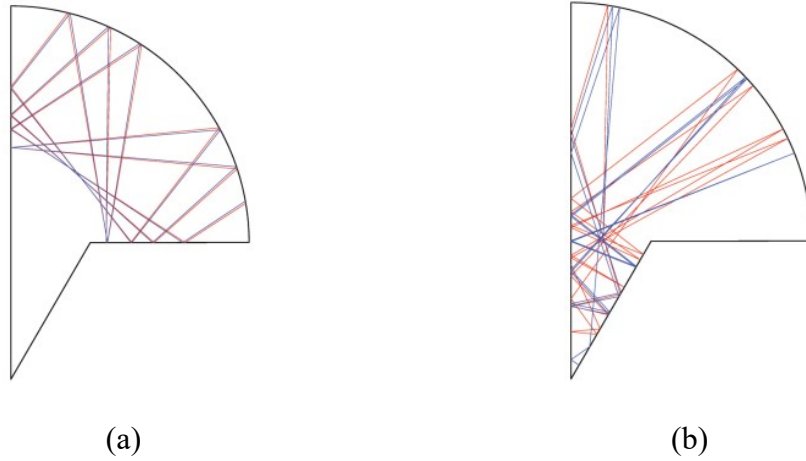


Figure 1.2: (a) Two regular ray trajectories in the Mushroom cavity, (b) Two chaotic ray trajectories in the Mushroom cavity.

The Mushroom cavity has been well studied [2, 3]. And we know the fact that the bottom triangular region of the Mushroom cavity is the “chaotic region”: only the chaotic ray trajectories will enter into the chaotic region (as shown in Fig. 1.2 (b)). While the upper quarter-circle region of the Mushroom cavity is the “regular region”: both regular and chaotic ray trajectories will enter into the regular region (as shown in Fig. 1.2). After long enough time, one chaotic ray trajectory will fill up the whole cavity, while one regular ray trajectory will be confined within the regular region.

If a cavity only has regular/chaotic ray trajectories in it, then it is a regular/chaotic system. If a cavity has both regular and chaotic ray trajectories coexisting in it, then it is a mixed system.

1.3.2 The RCM on Chaotic System Cavity Impedance

In my thesis, I will focus on studying the impedance of 2D cavity with ports. An illustration of a two-port 2D Mushroom cavity is plotted in Fig. 1.3 [3].

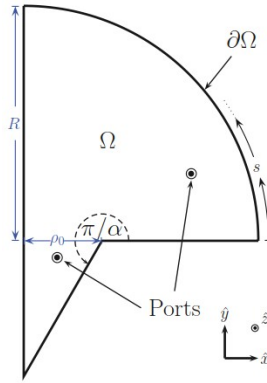


Figure 1.3: Two-port 2D Mushroom cavity

The wave equation for an M-port lossless cavity is [1-3]:

$$(\nabla^2 + k^2)\hat{V}_T = -jkh\eta_0 \sum_{j=1}^M u_j \hat{I}_j, \quad (1.11)$$

\hat{V}_T is the voltage difference between the top and bottom of the quasi-2D cavity, \hat{I}_j is the current at port j, u_j is the profile function of space at port j, η_0 is a constant, h is height of the cavity, and k is wave number,. Solving Eq. (1.11) for port voltages \hat{V}_i yields:

$$\hat{V}_i = \sum_{j=1}^M Z_{ij} \hat{I}_j, \quad (1.12)$$

where the impedance matrix \mathbf{Z} is given by:

$$Z_{ij} = -jkh\eta_0 \sum_{n=1}^N \frac{\langle u_i \phi_n \rangle \langle u_j \phi_n \rangle}{k^2 - k_n^2}, \quad (1.13)$$

where N satisfies the condition $2\pi/k_N \ll$ (*size of ports*), k_n is eigen wave number, ϕ_n is the n th eigenfunction of the cavity, and $\langle \dots \rangle = \int_{\Omega} \dots d^2\vec{x}$.

We can extract a dimensionless impedance from Eq. (1.13):

$$\zeta_{ij} = -\frac{1}{\pi} \sum_{n=1}^N \frac{\langle u_i \phi_n \rangle \langle u_j \phi_n \rangle}{\tilde{k}^2 - \tilde{k}_n^2}, \quad (1.14)$$

where $\tilde{k}^2 \equiv k^2/\Delta(k^2)$ is the normalized operating frequency, and $\tilde{k}_n^2 \equiv k_n^2/\Delta(k^2)$ is the system normalized eigenvalue.

so that:

$$Z_{ij} = j \frac{kh\eta_0}{4} \zeta_{ij}, \quad (1.15)$$

This new quantity “dimensionless impedance” is independent of system specific dimensions, and is therefore universal for all chaotic cavities.

The Random Coupling Model (RCM) is a model designed to analyze the radiation coupling of complicated enclosures through ports. If a system is pure chaotic, then the chaotic system will have all the nice wave chaos properties mentioned in section 1.2: Weyl’s formula for the normalized eigenvalue spacing, random matrix theory, and the random plane wave hypothesis. These properties support us to calculate the dimensionless impedance in Eq. (1.14) as following: insert the mean eigenvalue spacing as $\Delta(k^2) = 4\pi/A$, replace the eigenfunctions ϕ_n by Gaussian random variables in Eq. (1.10), and replace the normalized eigenvalues \tilde{k}_n^2 by the eigenvalues of GOE matrices. Note that in the RCM, we don’t need to actually

solve the chaotic system's eigenvalues and eigenfunctions. This is the very essence of the RCM.

1.3.3 The Generalized RCM on Mixed System Cavity Impedance

The RCM has been tested to be valid for pure chaotic system cavities in our group's previous work [1-3, 5, 6]. But for mixed system cavities which have coexisting regular and chaotic ray trajectories, we cannot apply RCM directly. Therefore we need to generalize the RCM first, and then apply the "generalized RCM" to study mixed system cavity impedance.

To generalize the RCM, we first need to decompose the mixed system cavity impedance \mathbf{Z} into contributions from the regular eigenmodes \mathbf{Z}_R and the chaotic eigenmodes \mathbf{Z}_C separately [3]:

$$\mathbf{Z} = \mathbf{Z}_R + \mathbf{Z}_C, \quad (1.16)$$

and $\mathbf{Z}_R, \mathbf{Z}_C$ are given by:

$$Z_{R,ij} = -jkh\eta_0 \sum_{r=1}^{N_R} \frac{\langle u_i \phi_r \rangle \langle u_j \phi_r \rangle}{k^2 - k_r^2}, \quad (1.17)$$

$$Z_{C,ij} = -jkh\eta_0 \sum_{c=1}^{N_C} \frac{\langle u_i \phi_c \rangle \langle u_j \phi_c \rangle}{k^2 - k_c^2},$$

where N_R/N_C is the total number of regular/chaotic eigenmodes, ϕ_r/ϕ_c is the regular/chaotic eigenfunction, k_r^2/k_c^2 is the regular/chaotic eigenvalue, and there should be $N_R + N_C = N$ eigenfunctions and eigenvalues.

After making decomposition of the mixed system cavity impedance \mathbf{Z} , we can apply the RCM to \mathbf{Z}_C following the same approach as solving a pure chaotic system cavity impedance, expect for there is a little difference: when replacing the chaotic

eigenfunctions ϕ_c by zero-mean Gaussian random variables, the variance $\sigma^2 = 1/A_C$ where A_C is the phase space area occupied by chaotic trajectories. While the Z_R is still calculated by solving eigenfunctions and eigenvalues of regular eigenmodes. This is how the generalized RCM treats the mixed system cavity impedance.

1.4 Outline of Thesis

In this thesis, I will focus on characterizing the dimensionless impedance of mixed systems by their probability density function. This thesis is organized as followed:

In Chapter 2, I discuss two types of mixed systems: the “Four Arcs” and the “Peanut” shaped boundary. I will employ the ray tracing method to study the trajectories inside these two systems. By plotting the trajectories in real space and in phase space, we can verify that both of these two systems are truly mixed systems, and they have rather complicated intermixed chaotic phase space regions and regular phase space regions.

In Chapter 3, I will implement the Method of Moments (MOM) to solve for the eigenfunctions and eigenvalues of our concerned 2D cavities. Derivation of the MOM algorithm formulas is also provided. As I already mentioned in this chapter, the eigenfunctions and eigenvalues are essential information for our generalized RCM. Besides, using numerical eigenfunctions and eigenvalues to calculate dimensionless impedance through the old deterministic method will give us good comparison with our RCM results.

In Chapter 4, I make a preliminary study applying the RCM to a two-port 2D rectangular cavity with Gaussian profile port function, first for the lossless case

second for a lossy case. I treat this regular system as if it were a chaotic system. The PDF of the dimensionless impedance calculated by the RCM and by using numerical eigenmodes are both given and compared.

In Chapter 5, I will make a summary of my work and discuss future work.

Chapter 2: Mixed System Billiard

A billiard is a 2D shaped region in which a particle moves following a trajectory defined by classical mechanics. The particle moves in a straight line at constant speed until it encounters the boundary where it reflects specularly, without losing any kinetic energy [2]. Depending on the shape of the boundary, the trajectories may be either be regular, chaotic or a mixture of regular and chaotic.

The billiard problem has a direct connection to the electromagnetic problem: when the EM wavelength is very small compared with the system dimensions, then EM waves will propagate inside the system very much like billiards. Mixed systems are those systems that have coexisting chaotic and regular billiard trajectories. To determine if a certain billiard shape is a mixed system or not, we can employ the ray tracing method to plot different billiard trajectories in both real space and phase space. In this chapter I will discuss two types of mixed systems: the “Four Arcs” and the “Peanut” billiard.

2.1 Four Arcs Billiard

2.1.1 Setup

The Four Arcs billiard is the first type of mixed system I study. In short, its boundary is four circular arcs of two different radii which together make a smooth elliptical-like shape. An illustration of the Four Arcs shape is shown in Fig. 2.1.

The Four Arcs boundary can be defined by this setup:

1. Specify the ratio of the two radii: r_1/r_2 . Without losing any generality, we can restrict this ratio to satisfy $r_1/r_2 \geq 1$.
2. Specify the value of the “top angle” $\psi \in (0, \pi)$. This is the angle of the two arcs having radii r_1 .
3. Adjust the size of r_1 and r_2 such that the enclosed area satisfies: $A = 4\pi$. Thus the average eigenvalue spacing will be unity (Weyl’s formula in 2D gives the average eigenvalue spacing to be: $\Delta(k^2) \equiv \langle k_{n+1}^2 - k_n^2 \rangle \simeq 4\pi/A$).

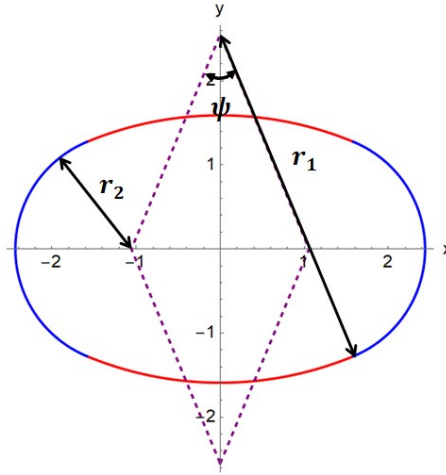


Figure 2.1: An illustration of Four Arcs setup, the two red arcs are of radius r_1 ; the two blue arcs are of radius r_2 . Connecting the four arcs’ centers by the dashed purple lines makes a rhombus. The “top angle” of the dashed purple rhombus is ψ .

Given the setup of the Four Arcs 2D billiard, once the quantities r_1/r_2 and ψ are specified while enforcing $A = 4\pi$, a valid Four Arcs boundary can be determined (there will always be real solutions for r_1 and r_2).

2.1.2 Four Arcs Billiard Trajectories in Real Space and in Phase Space

We can imagine in real space, we shoot a billiard with some initial position and angle inside the Four Arcs cavity, then the billiard will be bouncing back and forth inside the Four Arcs. Each time when the billiard bounces on the boundary, it obeys the law of specular reflection.

The Four Arcs billiard trajectory in phase space setup is plotted in Fig. 2.2. In Fig. 2.2, each bounce on the boundary can be recorded by a point in phase space: $(Scaled\ S, \cos\theta)$. Where S is the length from the “reference point” to the bounce point along the boundary, it is increasing in the counterclockwise direction. The “reference point” where $S = 0$ is at the bottom crossing point between Four Arcs and the y-axis. $Scaled\ S = S/perimeter\ of\ four\ arcs$, so $Scaled\ S \in [0,1]$. And θ is the vector angle between the billiard velocity direction vector at the bounce point, and the tangential vector along the counterclockwise direction. The vector angle θ is defined in such a way that the phase space $(Scaled\ S, \cos\theta)$ will be area preserving.

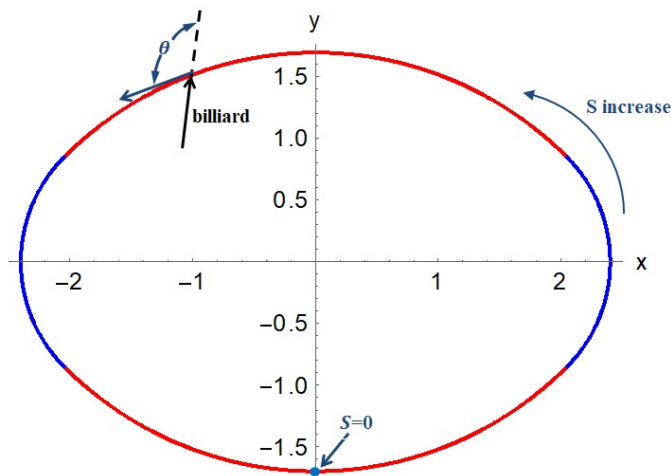


Figure 2.2: Four Arcs billiard phase space setup.

With the phase space setup being specified, we can now write a code to determine the billiard ray path. We can plot the Four Arcs billiard trajectory in real space and in phase space. As an example, in Fig. 2.3 I plot two billiard trajectories for the $r_1/r_2 = 1 + \sqrt{2}, \theta = \frac{\pi}{2}$ Four Arcs.

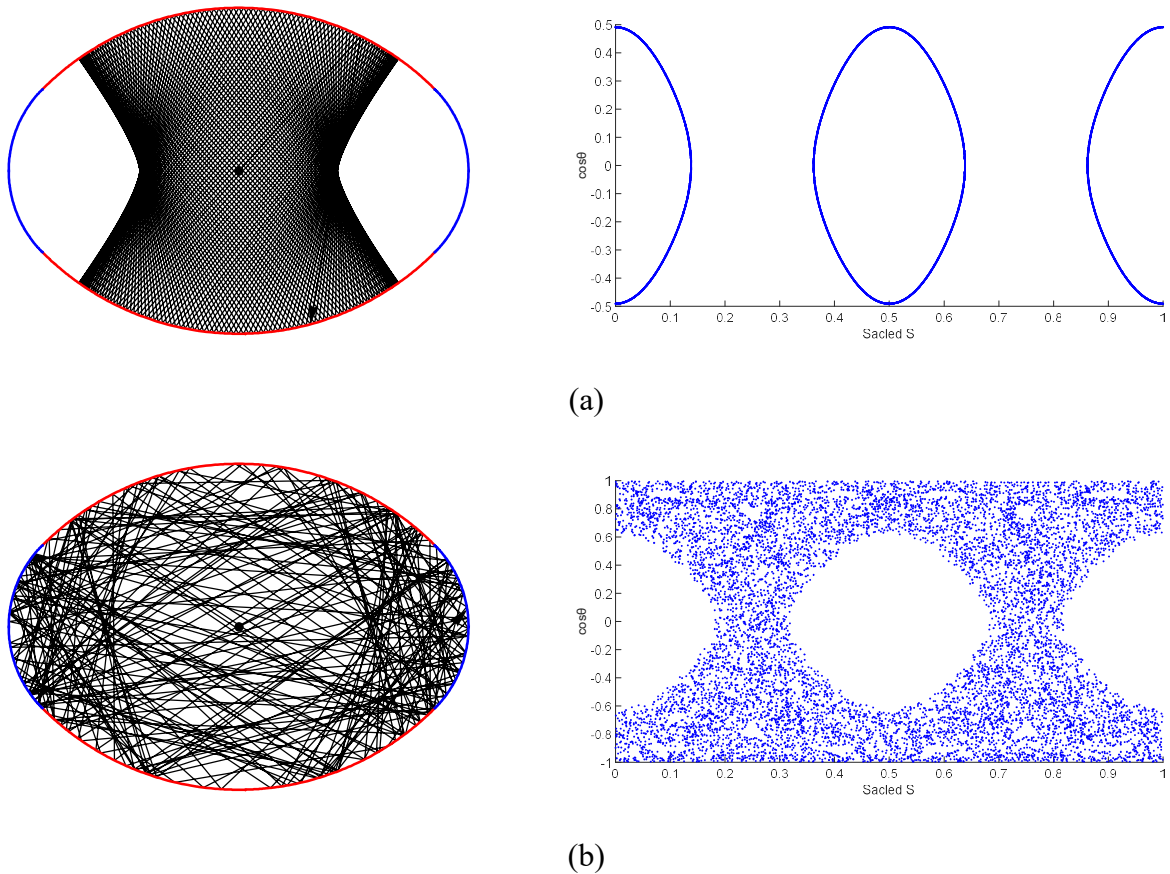


Figure 2.3: Real space trajectory (200 bounces) and the corresponding phase space trajectory (10,000 bounces) for the $r_1/r_2 = 1 + \sqrt{2}, \psi = \frac{\pi}{2}$ Four Arcs: (a) one regular trajectory, (b) one chaotic trajectory.

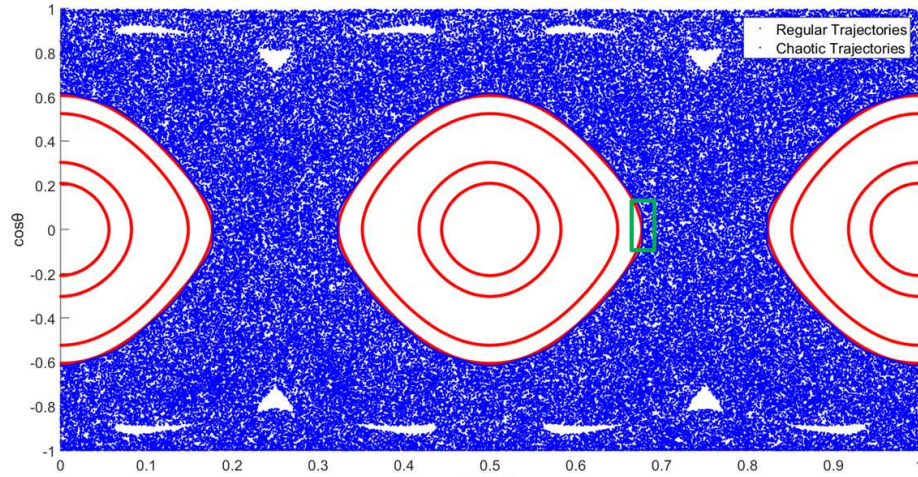
From Fig. 2.3, we can tell this $r_1/r_2 = 1 + \sqrt{2}, \psi = \frac{\pi}{2}$ Four Arcs is truly a mixed system. For some initial conditions (like in Fig. 2.3 (a)), the trajectories are confined

within a finite region in real space. We call these trajectories as “regular”. For these regular trajectories, their corresponding phase space trajectories are also confined to some “closed loops”. This kind of “closed loops” in phase space show that these regular trajectories are long term quasi-periodic with long enough time (large enough bounces times), trajectories will remain on the closed curve.

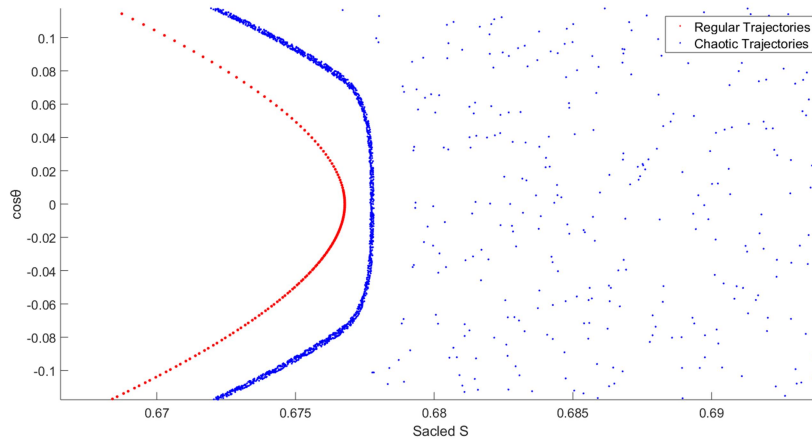
On the other hand, chaotic trajectories (like in Fig. 2.3 (b)) fill up real space: meaning a chaotic trajectory will eventually come close to any spatial point in the Four Arcs. In phase space however, it won’t take up the full phase space region. However the trajectory maps out an area in phase space. And it will enter most of the phase space region except for those regions reserved for regular trajectories. We call those blank regions that chaotic trajectories never enter “islands”, for they are surrounded by chaotic phase space regions.

Moreover, when we plot different regular and chaotic trajectories together in Fig. 2.4, the phase space plot will tell us even more about where the Four Arcs regular regions or “islands” are and where chaotic regions are. The boundary and relationship between regular regions and chaotic regions are easier to observe. The results clearly show that this $r_1/r_2 = 1 + \sqrt{2}, \psi = \frac{\pi}{2}$ Four Arcs is a mixed system.

By studying the billiard trajectories in both real space and phase space, we can determine if a certain shape of billiard is mixed system or not, and can distinguish between regular regions and chaotic regions.



(a)



(b)

Figure 2.4: (a) 4 regular trajectories (each 4,000 bounces, red dots) and 4 chaotic trajectories (each 40,000 bounces, blue dots) plotted together on the same phase space graph, (b) enlargement of the green rectangular box region in (a).

2.2 Peanut Billiard

2.2.1 Setup

The Peanut billiard is a different mixed system that I study. Its boundary is given in polar coordinates by:

$$\rho(\phi) = 1 + a \cos(2\phi), \quad (2.1)$$

where a is a constant: $a \in [0, 1]$.

The name ‘‘Peanut’’ comes from that the boundary shape very often looks like a peanut. An illustration of different Peanut boundary shapes is plotted in Fig. 2.5.

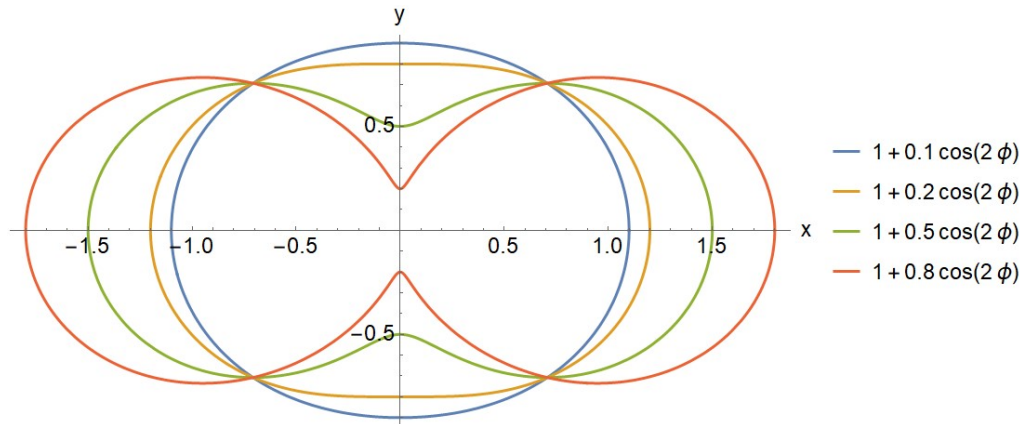


Figure 2.5: An illustration of different Peanut boundaries, with different parameters a values.

The enclosed area of the Peanut shape is given by

$$A = \int_0^{2\pi} \int_0^{1+a \cdot \cos(2\phi)} \rho d\rho d\phi, \quad (2.2)$$

which results in

$$A = \frac{\pi}{2} (2 + a^2), \quad (2.3)$$

The perimeter of the Peanut shape is given as follow:

$$\begin{aligned} \text{perimeter} &= \int_0^{2\pi} \sqrt{\rho^2 + \left(\frac{d\rho(\phi)}{d\phi}\right)^2} d\phi \\ &= \int_0^{2\pi} \sqrt{(1 + a \cdot \cos(2\phi))^2 + (-2a \cdot \sin(2\phi))^2} d\phi, \end{aligned} \quad (2.4)$$

Eq. (2.8) can be evaluated numerically.

It is worth pointing out that the tangential line slope at any given point (ρ_0, ϕ_0) on the Peanut boundary is:

$$\frac{dy}{dx} = \frac{-2a \cdot \sin(2\phi_0) \sin\phi_0 + \rho_0 \cos\phi_0}{-2a \cdot \sin(2\phi_0) \cos\phi_0 - \rho_0 \sin\phi_0}, \quad (2.5)$$

Eq. (2.5) is useful when you write a code to simulate the billiard reflects specularly on the Peanut shape boundary.

2.2.2 Peanut Billiard Trajectories in Real Space and in Phase Space

Following the same procedure as in the Four Arcs, the Peanut billiard trajectory in phase space setup is plotted in Fig. 2.6.

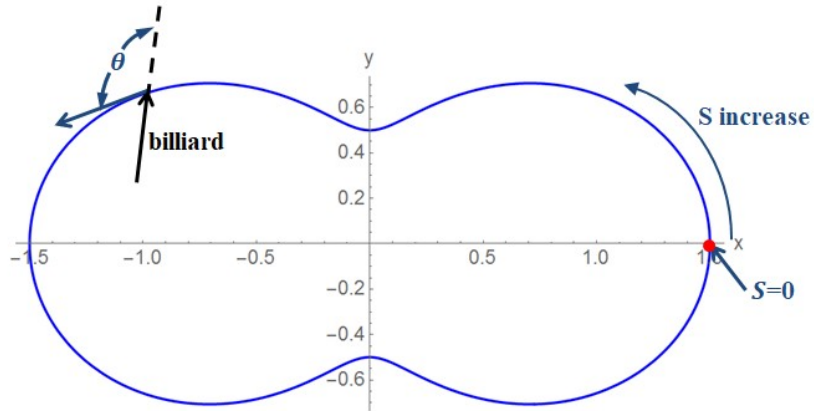
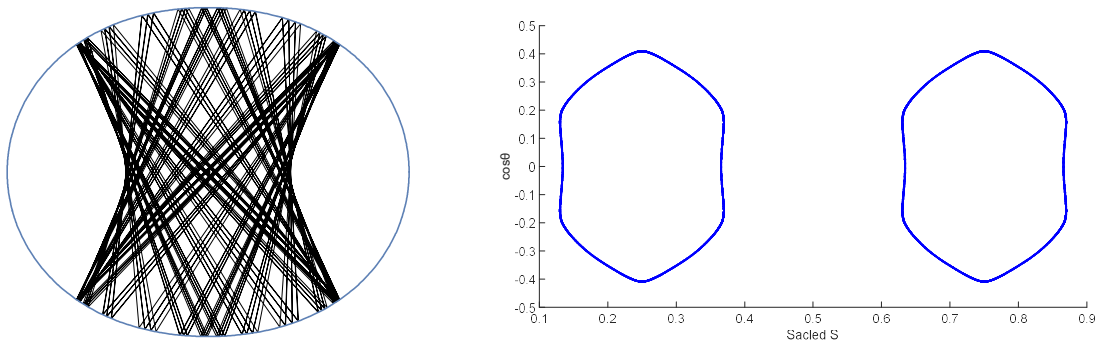


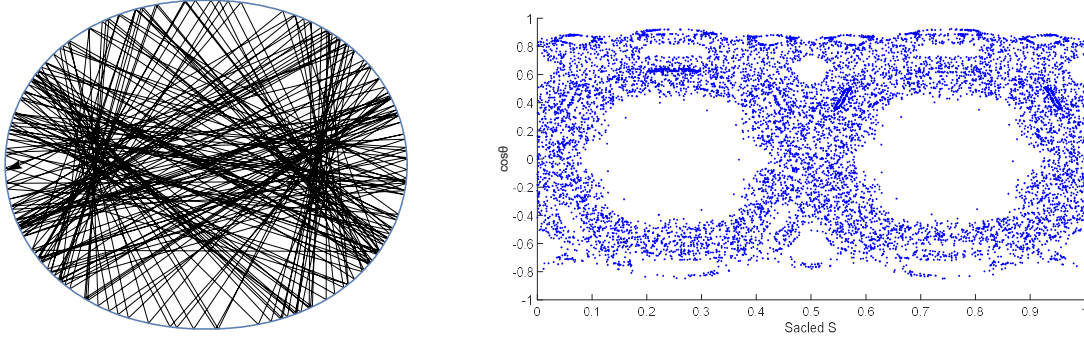
Figure 2.6: Peanut billiard phase space setup.

In Fig. 2.6, each bounce on the boundary can be recorded by a point in phase space: $(Scaled\ S, \cos\theta)$. Where S is the length from the “reference point” to the bounce point along the boundary, it is increasing in the counterclockwise direction. The “reference point” where $S = 0$ is at the right crossing point between Peanut boundary and the x-axis. $Scaled\ S = S/perimeter\ of\ Peanut$, so $Scaled\ S \in [0,1]$. And θ is the vector angle between the billiard velocity direction vector at the bounce point, and the tangential vector along the counterclockwise direction. The vector angle θ is defined in such a way that the phase space $(Scaled\ S, \cos\theta)$ will be area preserving.

Like what we did for the Four Arcs billiard in the previous section, we can now write a code to plot the Peanut billiard trajectory in real space and phase space. As an example, here I plot billiard trajectories for the $\rho(\phi) = 1 + 0.1 \cdot \cos(2\phi)$ Peanut cavity:



(a)

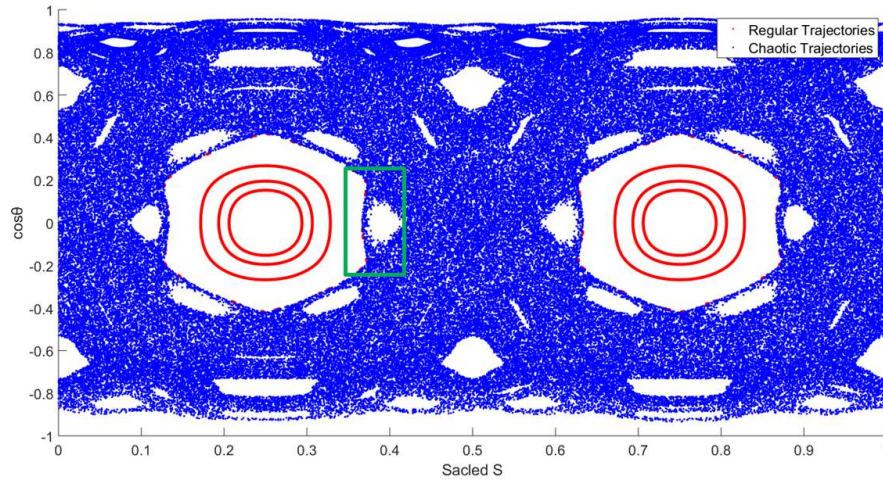


(b)

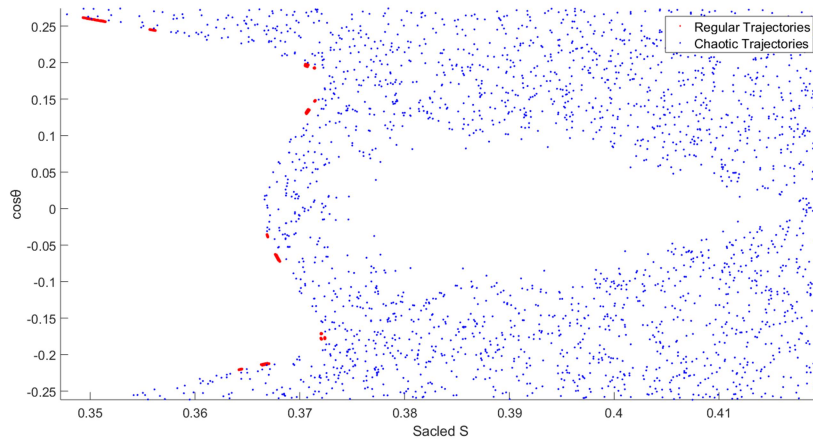
Figure 2.7: Real space trajectory (200 bounces) and corresponding phase space trajectory (10,000 bounces) for the $\rho(\phi) = 1 + 0.1\cos(2\phi)$ Peanut cavity: (a) one regular trajectory, (b) one chaotic trajectory.

Again, Fig. 2.7 clearly shows the $\rho(\phi) = 1 + 0.1\cos(2\phi)$ Peanut cavity is a mixed system. There are regular trajectories in this system (like in Fig. 2.6 (a)), and these regular trajectories will make “closed loops” in phase space, meaning they are long-term quasi-periodic. At the same time, there also are chaotic trajectories (like in Fig. 2.6 (b)). Chaotic trajectories will fill up real space, and take up some regions in phase space.

To further characterize the $\rho(\phi) = 1 + 0.1\cos(2\phi)$ Peanut cavity as a mixed system, we plot several different regular and chaotic trajectories in the phase space together in Fig. 2.8.



(a)



(b)

Figure 2.8: (a) 4 regular trajectories (each 4,000 bounces, red dots) and 4 chaotic trajectories (each 40,000 bounces, blue dots) plotted together on the same phase space graph, (b) enlargement of the green rectangular box region in (a).

Chapter 3: The Method of Moments on Eigenfrequencies and Eigenmodes of 2D Cavities

The Method of Moments (MOM), also known as the Boundary Element Method (BEM), is a powerful numerical technique to solve electromagnetic problems. Like the Finite Element Method (FEM), it will transform the continuous governing partial differential equation (in my case, it is the Helmholtz equation with zero potential on the boundary) in to a matrix equation. And then by solving the matrix equation, we can obtain the potential over the space, eigenfrequencies, eigenmodes and other kinds of electromagnetic information.

Compared with the FEM, there are some different properties of MOM [7-11]:

1. MOM only needs the information on the boundary to determine eigenvalues and eigenfunctions, not the information over the whole desired region/space. For example, when I'm studying 2D cavities, only points on the line boundary of the 2D cavity are needed to obtain the numerical solution. Thus the dimensionality of the problem is reduced by one by using MOM. The benefits of that are: (a) it's much faster and easier for MOM to discretize over a 1D contour than FEM to make meshes over a 2D cavity; (b) less information needs to be stored in the computer memory, meaning MOM is less likely to run into memory shortage than FEM.
2. For problems without a closed boundary, MOM will do better than FEM. This is because of that after MOM obtained the charge/potential distribution

on the boundary, even if that boundary is not closed, the outgoing wave radiation can be “automatically” achieved.

In this chapter, I will implement MOM to solve for Eigenfrequencies and Eigenmodes of the 2D cavities we are interested in. The numerical Eigenfrequencies and Eigenmodes will enable us to check if the Random Coupling Model gives the correct prediction of the cavity impedance probability distribution or not. And furthermore, the Eigenfrequencies and Eigenmodes information will help us to extend the Random Coupling Model predictions for Mixed Systems’ cavity impedance probability distribution.

3.1 Method of Moments in 2D Cavity Problems

3.1.1 Transform Homogenous Helmholtz Equation into Matrix Equation

The governing equation for a 2D cavity with a perfectly conducting metal wall is the homogenous Helmholtz equation:

$$(\nabla^2 + k^2)\varphi(\vec{x}) = 0, \quad \vec{x} \in \Omega, \quad (3.1)$$

where k is the wavenumber, Ω denotes the region inside a 2D cavity, and $\varphi(\vec{x})$ is the potential at position \vec{x} . The boundary condition to be applied to Eq. (3.1) is $\varphi(\vec{x}) = 0$ on the boundary.

Analytically, we know that the free-space Green’s function G_0 satisfies the homogenous Helmholtz equation

$$(\nabla^2 + k^2)G_0(\vec{x}, \vec{x}') = -\delta(\vec{x} - \vec{x}'), \quad (3.2)$$

The free-space Green’s function $G_0(\vec{x}, \vec{x}')$ is given by:

$$G_0(\vec{x}, \vec{x}') = \frac{1}{4j} H_0^{(2)}(k(\vec{x} - \vec{x}')), \quad (3.3)$$

where $H_0^{(2)}$ is the zeroth-order Hankel function of the second kind.

We multiply Eq. (3.1) by G_0 , and multiply Eq. (3.2) by φ on both sides, and then subtract the two results:

$$G_0 \nabla^2 \varphi - \varphi \nabla^2 G_0 = \varphi \delta(\vec{x} - \vec{x}'), \quad (3.4)$$

next we integrate Eq. (3.4) over the whole region inside the 2D cavity:

$$\iint_{\Omega} (G_0 \nabla^2 \varphi - \varphi \nabla^2 G_0) d\Omega = \iint_{\Omega} (\varphi \delta(\vec{x} - \vec{x}')) d\Omega, \quad (3.5)$$

We apply the second scalar Green's theorem

$$\iint_{\Omega} (G_0 \nabla^2 \varphi - \varphi \nabla^2 G_0) d\Omega = \oint_{\Gamma} \left(G_0 \frac{\partial \varphi}{\partial n} - \varphi \frac{\partial G_0}{\partial n} \right) d\Gamma, \quad (3.6)$$

where Γ is the boundary enclosing the 2D cavity region Ω .

Also, the right hand side of Eq. (3.5) is simply:

$$\iint_{\Omega} (\varphi(\vec{x}) \delta(\vec{x} - \vec{x}')) d\Omega = \varphi(\vec{x}'), \quad (3.7)$$

Next, we substitute Eq. (3.6) and (3.7) into Eq. (3.5), and the result is:

$$\oint_{\Gamma} \left(G_0 \frac{\partial \varphi}{\partial n} - \varphi \frac{\partial G_0}{\partial n} \right) d\Gamma = \varphi(\vec{x}'), \quad (3.8)$$

For a 2D cavity with perfect conducting metal wall, the boundary condition is:

$$\varphi(\vec{x}) = 0, \quad \vec{x} \in \Gamma, \quad (3.9)$$

with this boundary condition taken into account, and exchanging \vec{x} and \vec{x}' , Eq. (3.8)

will turn into:

$$\oint_{\Gamma'} G_0(\vec{x}, \vec{x}') \frac{\partial \varphi(\vec{x}')}{\partial n} d\Gamma' = 0, \quad \vec{x} \in \Gamma, \quad (3.10)$$

We can let $\frac{\partial \varphi(\vec{x}')}{\partial n} = \frac{1}{\varepsilon_0} \lambda(\vec{x}')$, and insert this into Eq. (3.10) :

$$\frac{1}{\varepsilon_0} \oint_{\Gamma} G_0(\vec{x}, \vec{x}') \lambda(\vec{x}') d\Gamma' = 0, \quad \vec{x} \in \Gamma, \quad (3.11)$$

where ε_0 is the vacuum permittivity constant, and $\lambda(\vec{x}')$ is the line charge density on the boundary.

So far, I have finished the derivation of transforming the homogenous Helmholtz equation (Eq. (3.1)), with zero potential on the boundary, into an integral equation (Eq. (3.11)). Next I'm going to transform the integral equation Eq. (3.11) into a matrix equation.

If I discretize the boundary of a 2D cavity into N segments, and approximate the contour integral by the sum of N integrals over each small segments:

$$\frac{1}{\varepsilon_0} \oint_{\Gamma} G_0(\vec{x}, \vec{x}') \lambda(\vec{x}') d\Gamma' \approx \frac{1}{\varepsilon_0} \sum_{n=1}^N Z_{mn} \lambda_n = \varphi_m = 0, \quad (3.12)$$

where m, n are just dummy indices to mark the segments. And Z_{mn} is given by:

$$Z_{mn} = \int_{s_n} G_0(\vec{x}_m, \vec{x}'_n) d\Gamma', \quad (3.13)$$

where s_n is the length of the nth segment. Z_{mn} is a $N \times N$ coefficient matrix.

In the end, Eq. (3.12) is the homogenous matrix equation we transformed from the homogenous Helmholtz equation. We can write a code to numerically solve this homogenous matrix equation on a computer. The eigenvalues of matrix Z_{mn} will tell us the eigenfrequencies of the 2D cavity. And the eigenvectors λ_n will tell us the line charge density distribution on the cavity boundary from which the solution in the interior can be found. Furthermore the eigenmodes potential distribution inside the

2D cavity can be achieved by simply implementing Green's function, once we have obtained line charge density vector λ_n .

3.1.2 Evaluate the Coefficient Matrix of the Helmholtz Matrix Equation

In this section of my thesis, I will evaluate and give formulas for the elements of \mathbf{Z} coefficient matrix.

First it is quite obvious that, when $m \neq n$, the Z_{mn} integral can be approximated by:

$$\begin{aligned} Z_{mn} &= \int_{s_n} G_0(\vec{x}_m, \vec{x}'_n) d\Gamma' \approx s_n \cdot G_0(\vec{x}_m, \vec{x}'_n) \\ &= \frac{s_n}{4} H_0^{(2)}(k|\vec{x}_m - \vec{x}'_n|), \quad m \neq n, \end{aligned} \quad (3.14)$$

The real question is when $m = n$. As $|\vec{x}_m - \vec{x}'_n|$ becoming zero, then it takes some special treatment to evaluate Z_{mn} . We call the " Z_{mn} , $m = n$ " as the "self-term".

For the self-terms, we study them in the polar coordinates, and imagine there is a circle of radius r contouring the self-term segment. Therefore,

$$\begin{aligned} |\vec{x}_m - \vec{x}'_n| &= |\vec{x}(\theta) - \vec{x}(\theta')| = |2r^2 - 2r^2 \cos(\theta - \theta')| \\ &= \sqrt{2}r \cdot \sqrt{1 - \cos(\theta - \theta')} \approx \sqrt{2}r \cdot \sqrt{\frac{1}{2}(\theta - \theta')^2}, \quad m = n, \end{aligned} \quad (3.15)$$

Insert this Eq. (3.15) into the Z_{mn} integral, then we have:

$$Z_{mn} \approx \frac{1}{4} \int_{\theta' - \frac{\Delta\theta}{2}}^{\theta' + \frac{\Delta\theta}{2}} H_0^{(2)} \left(kr \sqrt{\frac{1}{2}|\theta - \theta'|} \right) r d\theta', \quad m = n, \quad (3.16)$$

and since the Taylor expansion of the $H_0^{(2)}$ tells us that:

$$H_0^{(2)}(x) \approx 1 - i \frac{2}{\pi} \left[\ln \left(\frac{x}{2} \right) + \gamma \right], \quad \text{when } x \rightarrow 0, \quad (3.17)$$

where γ is a constant called ‘‘Euler Gamma’’, $\gamma \approx 0.577216$.

Apply the approximation in Eq. (3.17) to Eq. (3.16), and set $\theta' = 0$, we get:

$$\begin{aligned} Z_{mn} &\approx \frac{1}{4} r \int_{-\frac{\Delta\theta}{2}}^{\frac{\Delta\theta}{2}} \left\{ 1 - i \frac{2}{\pi} \left[\ln \left(\frac{1}{2} kr |\theta'| \right) + \gamma \right] \right\} d\theta' \\ &= \frac{1}{4} r \Delta\theta \left\{ 1 - i \frac{2}{\pi} \left[\ln \left(\frac{1}{2} kr \right) + \gamma \right] \right\} - \frac{1}{4} r \int_{-\frac{\Delta\theta}{2}}^{\frac{\Delta\theta}{2}} i \frac{2}{\pi} \ln(|\theta'|) d\theta', \quad m = n, \end{aligned} \quad (3.18)$$

The integral part of the equation can be evaluated:

$$\int_{-\frac{\Delta\theta}{2}}^{\frac{\Delta\theta}{2}} \ln(|\theta'|) d\theta' = 2 \int_0^{\frac{\Delta\theta}{2}} \ln(|\theta'|) d\theta' = \Delta\theta \left[\ln \left(\frac{\Delta\theta}{2} \right) - 1 \right], \quad (3.19)$$

Insert Eq. (3.19) into Eq. (3.18), and recall that in polar coordinates $r\Delta\theta = s_n$, we get:

$$\begin{aligned} Z_{mn} &\approx \frac{1}{4} r \Delta\theta \left\{ 1 - i \frac{2}{\pi} \left[\ln \left(\frac{1}{2} kr \right) + \gamma \right] - i \frac{2}{\pi} \left[\ln \left(\frac{\Delta\theta}{2} \right) - 1 \right] \right\} \\ &= \frac{s_n}{4} \left[1 - i \frac{2}{\pi} \ln \left(\frac{ke^\gamma s_n}{4e} \right) \right], \quad m = n, \end{aligned} \quad (3.20)$$

where $e^\gamma \approx 1.78107$.

In sum, the coefficient matrix Z_{mn} for our homogenous Helmholtz matrix equation is evaluated by these formulas [7]:

$$Z_{mn} = \begin{cases} \frac{s_n}{4} H_0^{(2)}(k|\vec{x}_m - \vec{x}_n|), & m \neq n \\ \frac{s_n}{4} \left[1 - i \frac{2}{\pi} \ln \left(\frac{ke^\gamma s_n}{4e} \right) \right], & m = n, \end{cases} \quad (3.21)$$

where k is the wave number, s_n is the uniform segment length on the boundary,

$e \approx 2.7183$, $e^\gamma \approx 1.78107$.

3.1.3 Solve the Homogenous Helmholtz Equation Numerically

As we can see in Eq. (3.21), the coefficient matrix \mathbf{Z} is a function of wave number k . So the homogenous Helmholtz equation we are trying to solve reduces to:

$$\mathbf{Z}(k) \cdot \vec{\lambda} = 0, \quad (3.22)$$

where $\vec{\lambda}$ is the line charge density on each segment stored in vector form. The wave numbers k that satisfy this above equation and their corresponding line charge density vectors $\vec{\lambda}$ are the unknowns we are trying to determine.

Technically, Eq. (3.22) only has non-trivial solution when the determinant of \mathbf{Z} matrix is zero: $\text{Det}[\mathbf{Z}(k)] = 0$. However, numerically it is almost impossible to find a k value which makes the determinant strictly zero. Instead, the best result a computer can achieve is to find some k values which make: $\text{Det}[\mathbf{Z}(k)] = \varepsilon \approx 0$.

With the reason given above, the actual numerical solver work flow is:

1. Find special k values: k_0 , so that at these k_0 we have: $\text{Det}[\mathbf{Z}(k_0)] = \varepsilon \approx 0$.
2. For each k_0 we found, we can calculate this eigen-problem:

$$\mathbf{Z}(k_0) \cdot \vec{\lambda}_{min} = a_{min} \cdot \vec{\lambda}_{min}, \quad (3.23)$$

where a_{min} denotes the smallest eigenvalue of $\mathbf{Z}(k_0)$, and $\vec{\lambda}_{min}$ is its corresponding eigenvector.

3. Numerically and practically, k_0 is the eigen wave number we are looking for.

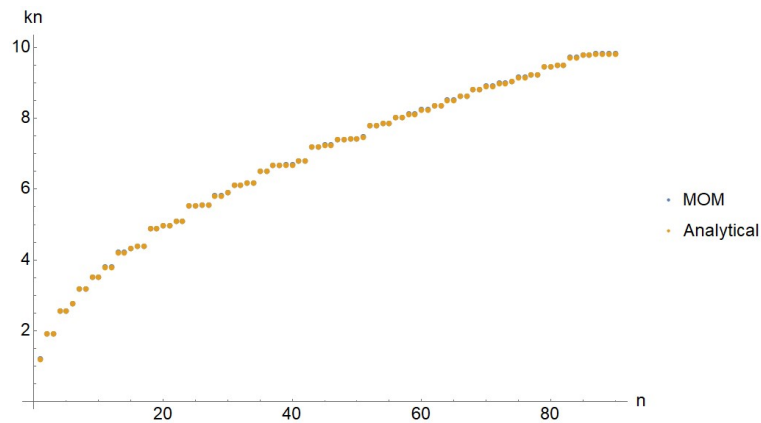
And $\vec{\lambda}_{min}$ is the charge density distribution on the boundary for an eigenmode. k_0 will tell us about the eigenfrequencies of the 2D cavity, and eigenmodes can be reproduced by implementing Green's function with $\vec{\lambda}_{min}$.

3.2 Implement the Method of Moments on the Circular, the Four Arcs and the Peanut Cavities

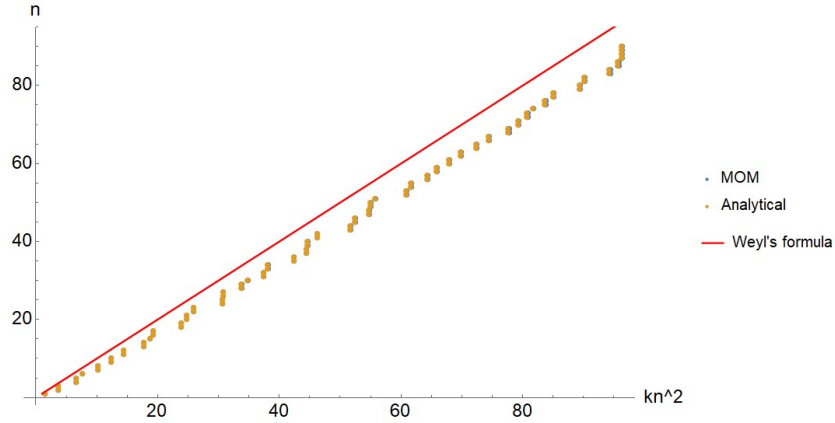
3.2.1 Eigenfrequencies and Eigenmodes of the Circular Cavity

We start to implement the algorithm we derived in section 3.1 by solving for a circular cavity. Since circular cavities have well-known analytical solutions (TM modes solution in our zero potential on the boundary case), we test if our algorithm can work or not.

For a $r=2$ circular cavity, the enclosed area is $A = 4\pi$. Plot the eigen wave numbers k_0 we found by using MOM vs. the analytical eigen wave numbers, in the range of $k \in [1, 10]$ in Fig. 3.1.



(a)



(b)

Figure 3.1: $r = 2, A = 4\pi$ circular cavity (a) k_n vs. n , MOM results (blue dots) vs. Analytical (yellow dots), and (b) n vs. k_n^2 , MOM results (blue dots), Analytical results (yellow dots), and Weyl's formula $n = \frac{A}{4\pi} k_n^2 = k_n^2$ (red line); where $k_n \in [1, 10]$.

As we can see in Fig. 3.1, the k_0 found by MOM are very close to the analytical k_0 , therefore the blue dots and the yellow dots are almost on top of each other. This shows that our MOM algorithm can work. The maximum absolute difference in the above figure is roughly 0.01, and the maximum percent error is roughly 0.13%.

We can also solve for the eigenmodes. A plot density φ^2 of selected eigenmodes of an $r=2$ circular cavity is shown in Fig. 3.2.

It's worth mentioning that even though my MOM code works well in finding most of the eigenfrequencies and eigenmodes, on the other hand there will be some eigenmodes missing. This missing eigenmodes problem is mainly due to the circular cavity being a regular system, and there is no "level repulsion" in its eigenvalues spectrum. In other words, two adjacent eigenfrequencies (eigenvalues) of a circular cavity can be infinitely close with each other. As I mentioned in Chapter 1, the PDF

of eigenvalues for a regular system should obey the Poisson distribution, as plotted in Fig. 3.3.

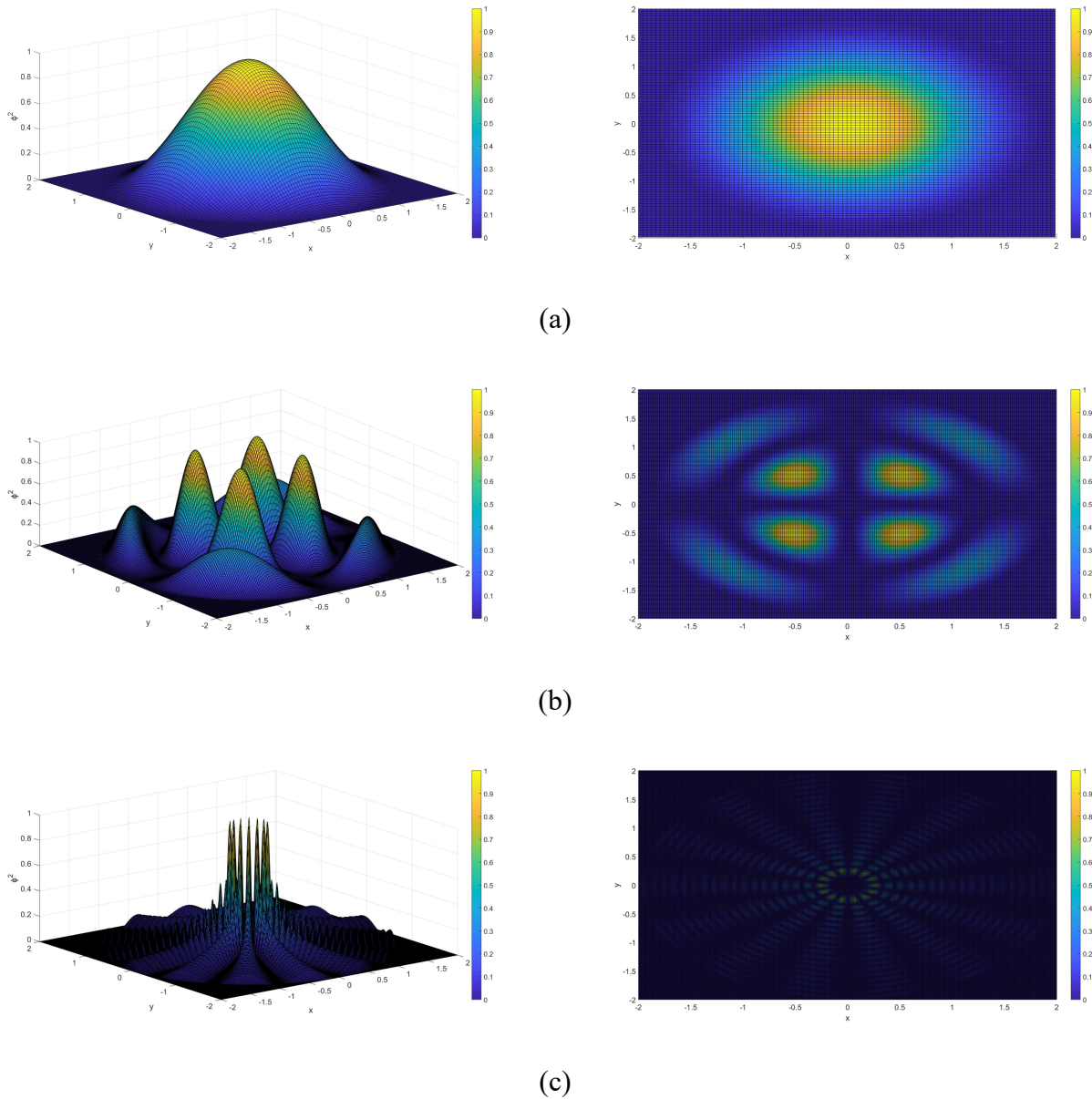


Figure 3.2: φ^2 density plot (3D view and top view) of three different eigenmodes for a $r=2$ circular cavity: (a) when $k_0 = 1.204$ (TM(0, 1)), (b) when $k_0 = 4.214$ (TM(2, 2)), and (c) when $k_0 = 33.1992$ (TM(16, 14)).

The numerical solver, with some approximations it already takes (see section 3.1), plus the limitation in computational resources, cannot tell the difference between two very close adjacent eigenmodes. That's why my MOM numerical solver will miss finding some eigenmodes. After tuning my code, I found 2390 out of the first 2456 eigenmodes of the $r=2$ circular cavity. So 2.69% of the eigenmodes are missing. We can assume the same accuracy also applies to other types of regular systems or the regular eigenmodes of mixed systems.

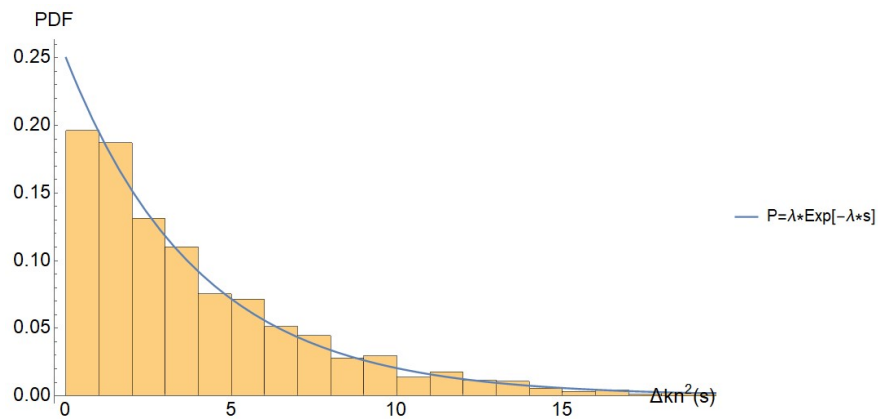


Figure 3.3: The eigenvalues spacing of an $r=2$ circular cavity, roughly 2500 eigenmodes histogram vs. Poisson distribution function (blue line).

3.2.2 Eigenfrequencies and Eigenmodes of the Four Arcs Cavity

Following the same steps as in the circular cavity problem, we can write a code to compute the eigenfrequencies and eigenmodes of the Four Arcs cavities. In this section, I will use the setup of: $r_1/r_2 = 1 + \sqrt{2}$, $\theta = \frac{\pi}{2}$ and the enclosed area is $A = 4\pi$ for the Four Arcs we study.

Plot the first 90 eigen wave numbers (in the range of $k \in [1, 10]$) the MOM numerical solver obtained in Fig. 3.4. Unlike in the circular cavity case, this time we don't have any analytical results to compare with.

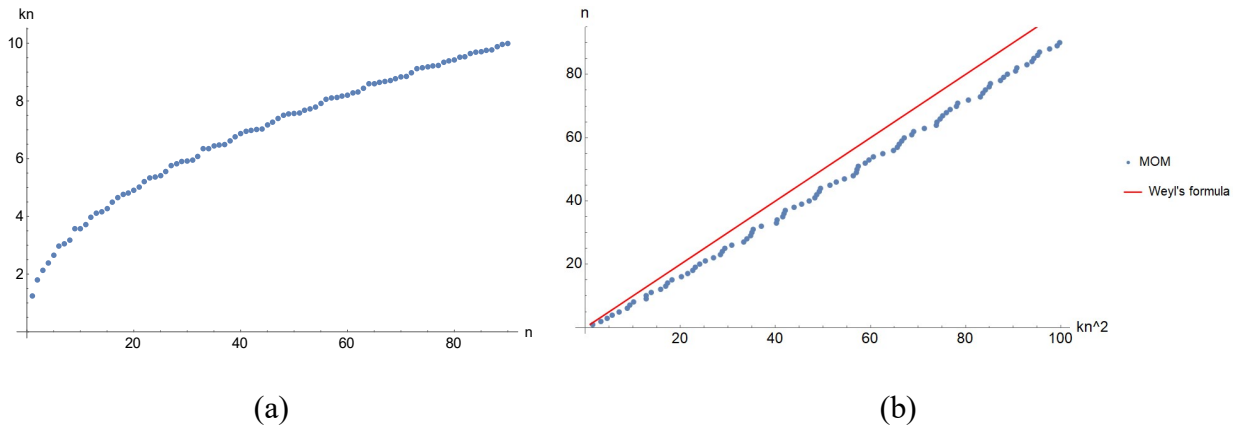
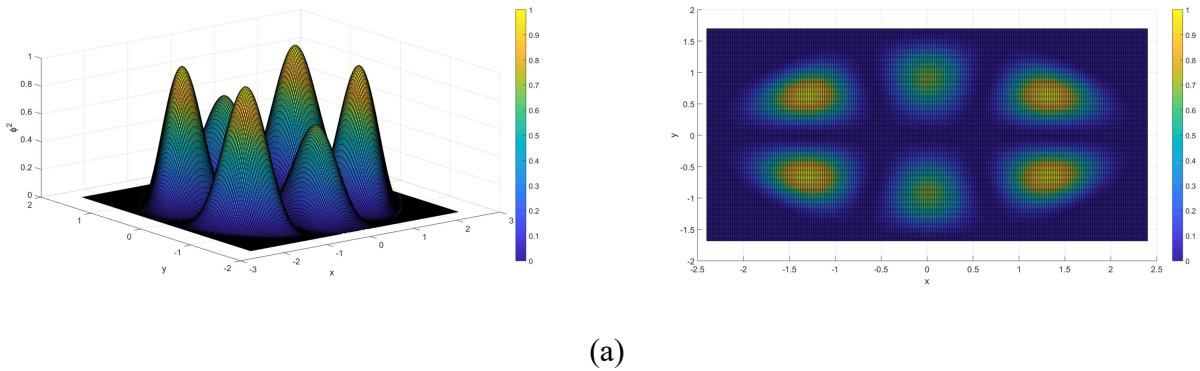
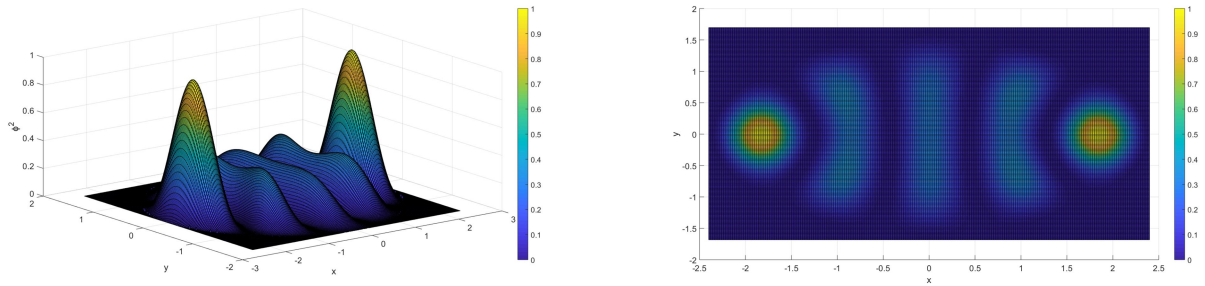


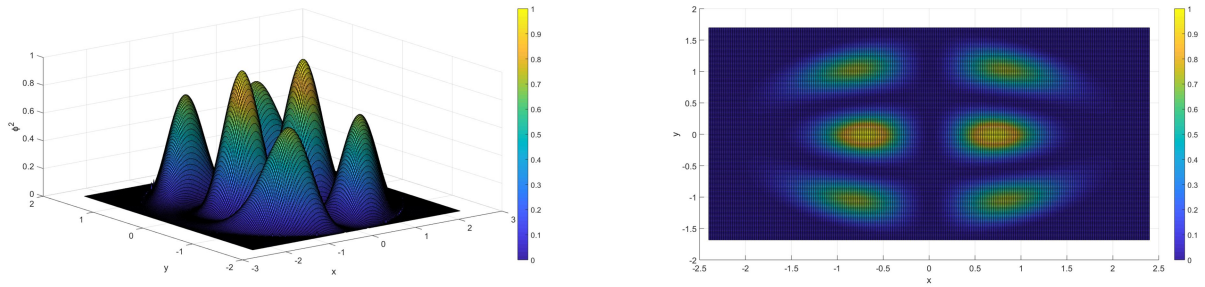
Figure 3.4: $r_1/r_2 = 1 + \sqrt{2}$, $\theta = \frac{\pi}{2}$ Four Arcs cavity (a) k_n vs. n of MOM results, and (b) n vs. k_n^2 , MOM results (blue dots) vs. Weyl's formula $n = \frac{A}{4\pi} k_n^2 = k_n^2$ (red line); where $k_n \in [1, 10]$.

We can solve for the eigenmodes for this $r_1/r_2 = 1 + \sqrt{2}$, $\theta = \frac{\pi}{2}$ Four Arcs cavity and plot three consecutive low order eigenmodes in Fig. 3.5.





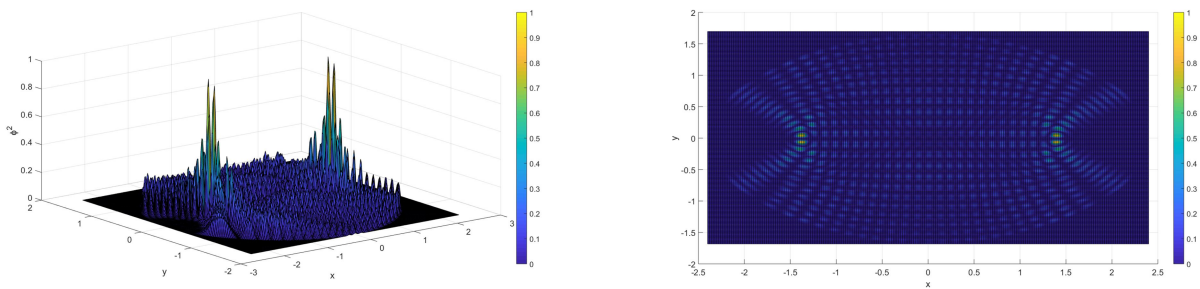
(b)



(c)

Figure 3.5: φ^2 density plot (3D view and top view) of 8th~10th eigenmodes for the $r_1/r_2 = 1 + \sqrt{2}$, $\theta = \frac{\pi}{2}$ Four Arcs cavity: (a) when $k_n = 3.183$ (n=8), (b) when $k_n = 3.568$ (n=9), and (c) when $k_n = 3.572$ (n=10).

We can also go further to increase eigen wave number k_n , and solve for eigenmodes again. Plot the results for three consecutive higher order eingemodes in Fig. 3.6.



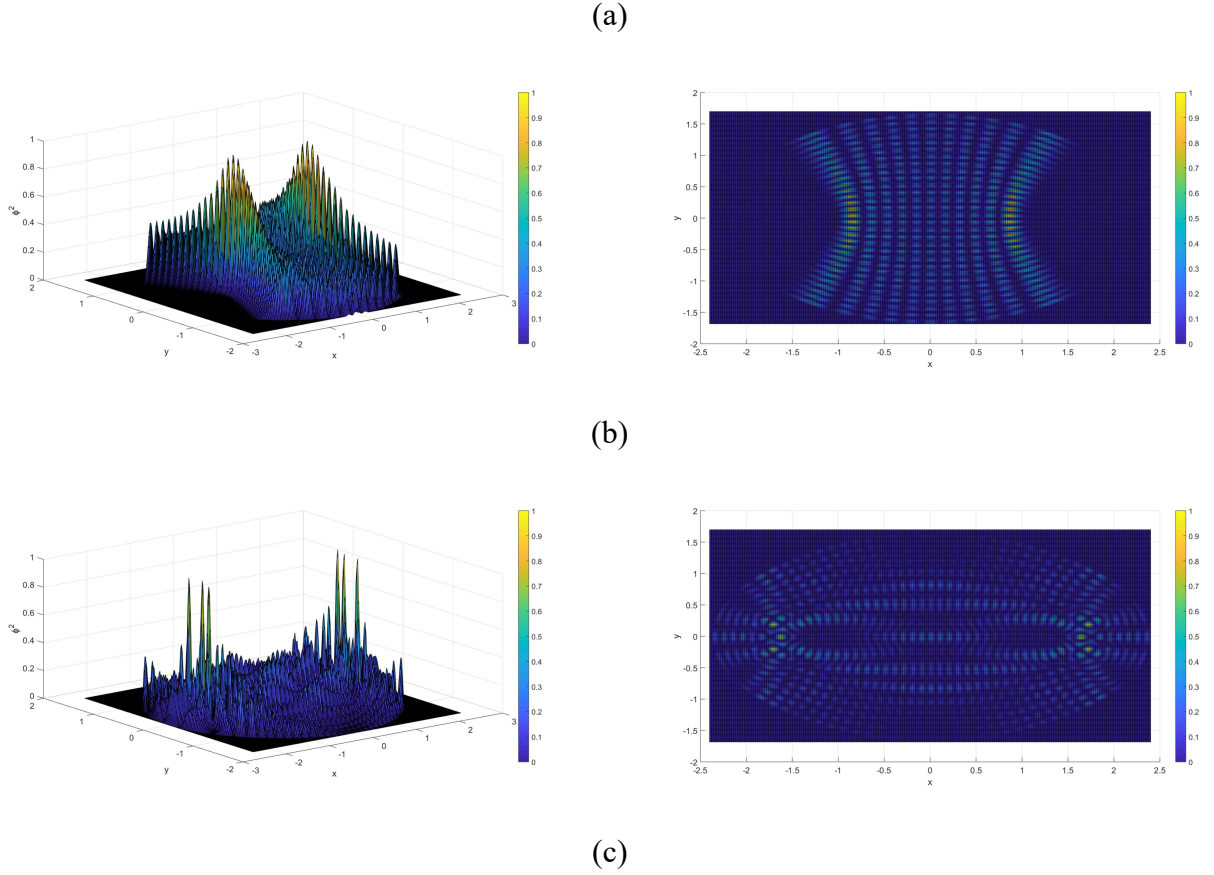


Figure 3.6: φ^2 density plot (3D view and top view) of three consecutive eigenmodes at $n \approx 1100$ for the $r_1/r_2 = 1 + \sqrt{2}$, $\theta = \frac{\pi}{2}$ Four Arcs cavity: (a) when $k_n = 33.2022$, (b) when $k_n = 33.2052$, and (c) when $k_n = 33.2172$.

3.2.3 Eigenfrequencies and Eigenmodes of the Peanut Cavity

In this section, we will use MOM code to solve for the eigenfrequencies and eigenmodes of Peanut cavity, with the boundary given by this function: $\rho(\phi) = 1 + 0.1\cos(2\phi)$, enclosed area $A = \frac{201}{200}\pi$.

First use the MOM solver to get the first 90 eigen wave numbers (in the range of $k_n \in [1, 20]$), and plot them in Fig. 3.7.

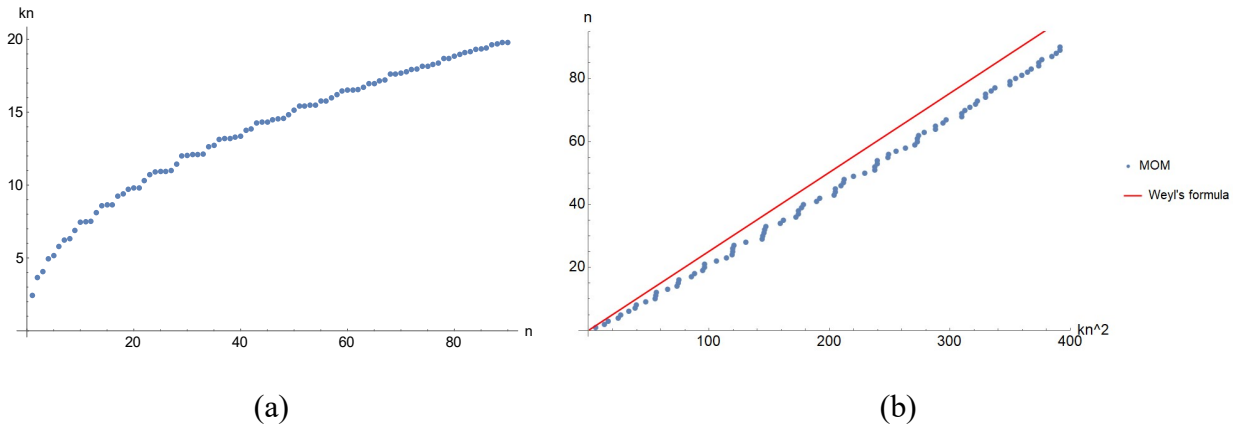
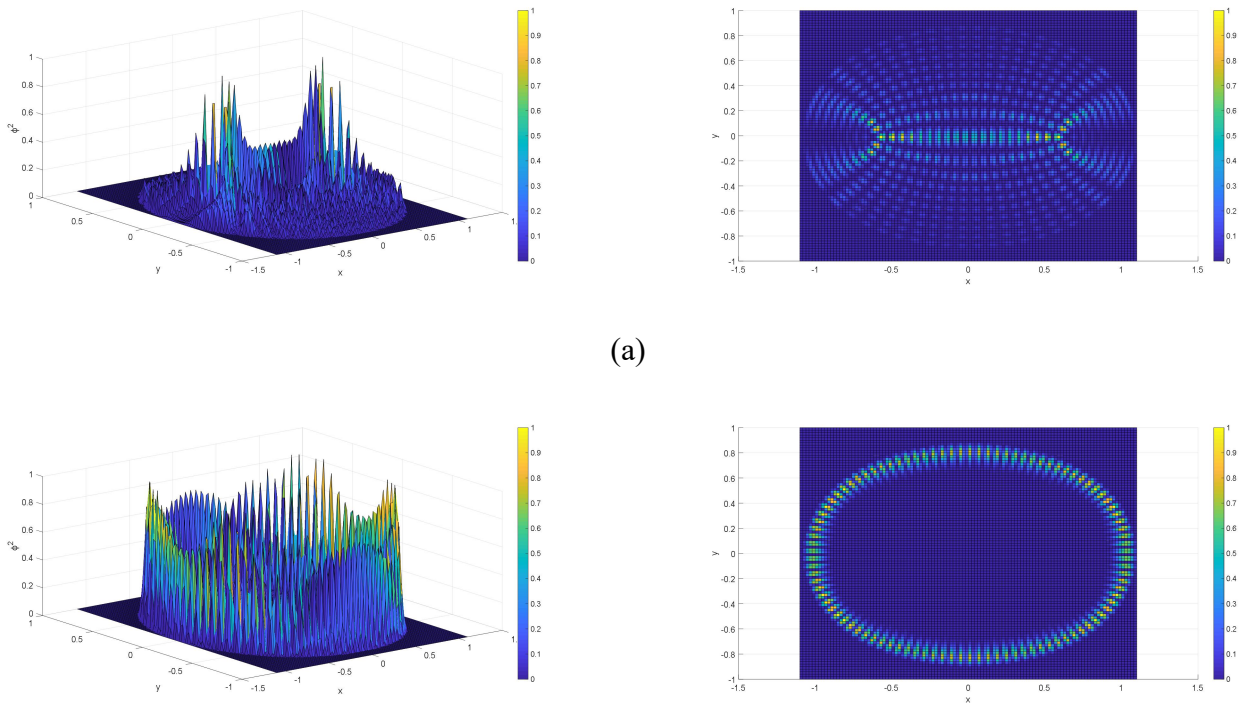
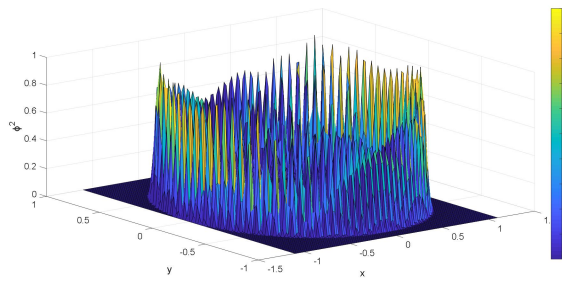


Figure 3.7: $\rho(\phi) = 1 + 0.1\cos(2\phi)$, $A = \frac{201}{200}\pi$ Peanut cavity (a) MOM k_n vs. n , and (b) n vs. k_n^2 , MOM numerical results (blue dots) and Weyl's formula $n = \frac{A}{4\pi}k_n^2 = 0.25125k_n^2$ (red line); where $k_n \in [1, 20]$.

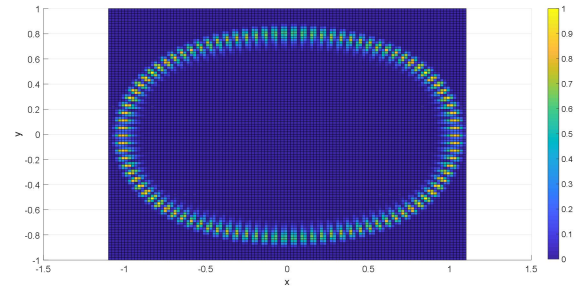
Solve for four consecutive high order eigenmodes of this Peanut cavity, and plot them in Fig. 3.8.



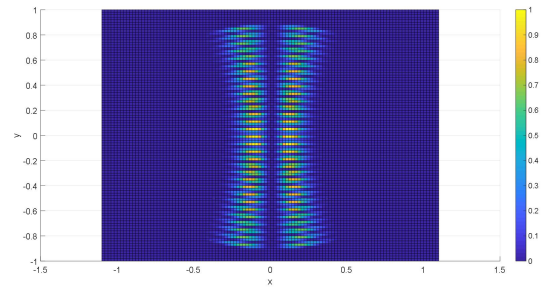
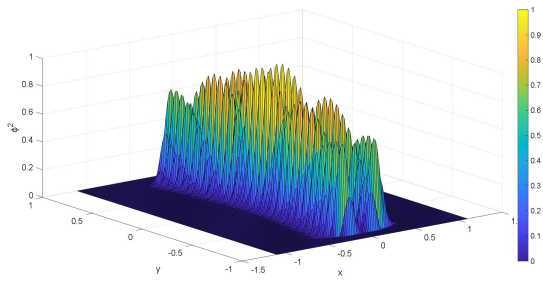
(a)



(b)



(c)



(d)

Figure 3.8: φ^2 density plot (3D view and top view) of four consecutive eigenmodes at $n \approx 766$ for the $\rho(\phi) = 1 + 0.1\cos(2\phi)$, $A = \frac{201}{200}\pi$ Peanut cavity: (a) when $k_n = 53.4668$, (b) when $k_n = 53.4788$, (c) when $k_n = 53.4788$, and (d) when $k_n = 53.5478$.

Chapter 4: Statistical Study of a Two-Port 2D Rectangular Cavity Impedance

4.1 Setup

The setup of rectangular cavity with two ports is plotted in Fig. 4.1. In my study, I choose these values for parameters:

$$\begin{cases} r_1 = r_2 = 0.01 \\ a = \frac{1 + \sqrt{5}}{2}, \quad b = 1 \\ (x_1, y_1) = (0.3, 0.8), \quad (x_2, y_2) = (1.2, 0.4), \end{cases} \quad (4.1)$$

where r_1, r_2 denotes the radius of port 1 and 2, a and b are the length of the rectangular edges, (x_1, y_1) and (x_2, y_2) are the center positions of the two port 1 and 2. The $(0,0)$ coordinate is at the bottom left corner of the rectangular. The reason of why we are choosing these values for parameters will be explained later in the next section, when we derive formulas for cavity impedance.

The profile functions of the two ports are Gaussian profile functions:

$$u_{1,2} = \frac{1}{2\pi r_{1,2}^2} \text{Exp} \left[-\frac{(x - x_{1,2})^2 + (y - y_{1,2})^2}{2r_{1,2}^2} \right], \quad (4.2)$$

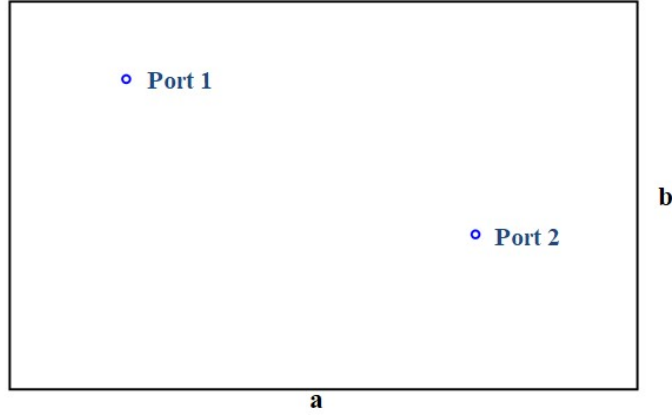


Figure 4.1: The setup of the rectangular box with two ports.

4.2 Impedance for Lossless Two-Port 2D Rectangular Cavity

4.2.1 Formulas for Lossless Impedance

I will first derive the formula for lossless impedance for a rectangular cavity with two Gaussian profile function ports.

For a lossless cavity with M ports, the impedance matrix \mathbf{Z} is given by [1-3]:

$$Z_{ij} = -jkh\eta_0 \sum_{n=1}^N \frac{\langle u_i \phi_n \rangle \langle u_j \phi_n \rangle}{k^2 - k_n^2}, \quad (4.3)$$

where N satisfies the condition $2\pi/k_N \ll r_{1,2}$, in our case we choose N =6347 (the reason will be explained later after we derived the impedance formulas). Moreover, $k = \omega/c$, $\eta_0 = \sqrt{\mu_0/\epsilon_0}$, h is the height of the cavity (very small, virtually 2D cavity), and $\langle u_i \phi_n \rangle = \int_{\Omega} u_i \phi_n d^2\vec{x}$ is the integral over the whole region of profile function at port i (u_i) times the nth eigen-function (ϕ_n).

For lossless cavity, the impedance is purely imaginary. According to previous work [1-3], we can write the lossless impedance matrix into:

$$\mathbf{Z} = j \frac{kh\eta_0}{4} \mathbf{\Xi}, \quad (4.4)$$

where $\mathbf{\Xi}$ is the dimensionless reactance matrix:

$$\mathbf{\Xi} = -\frac{1}{\pi} \sum_n \frac{\mathbf{w}_n \mathbf{w}_n^T}{\tilde{k}^2 - \tilde{k}_n^2}, \quad (4.5)$$

in which $\tilde{k}^2 = \frac{k^2}{\Delta(k^2)} = \frac{k^2}{4\pi/A}$, where $\Delta(k^2) = 4\pi/A$ is the mean eigenvalue spacing for a 2D cavity, and the vector \mathbf{w}_n is defined by:

$$[\langle u_1 \phi_n \rangle, \dots, \langle u_M \phi_n \rangle]^T \equiv \frac{1}{\sqrt{A}} \mathbf{w}_n, \quad (4.6)$$

In the end, the dimensionless reactance matrix in Eq. (4.5) is the value we are calculating.

To evaluate Eq. (4.5) numerically, we need to insert the numerical eigenvalues and eigenfunctions of the rectangular box, and the profile functions Eq. (4.2).

Combining these together, we get:

$$\begin{aligned} \Xi_{ij} = & -\frac{16}{A} \sum_{n=1}^N \text{Exp} \left[-\frac{1}{2} k_n^2 (r_i^2 + r_j^2) \right] \cdot \sin \left(\frac{n_x \pi}{a} x_i \right) \sin \left(\frac{n_y \pi}{b} y_i \right) \\ & \cdot \sin \left(\frac{n_x \pi}{a} x_j \right) \sin \left(\frac{n_y \pi}{b} y_j \right) / (k^2 - k_n^2), \quad (4.7) \\ & k_n^2 = \left(\frac{n_x \pi}{a} \right)^2 + \left(\frac{n_y \pi}{b} \right)^2, \end{aligned}$$

As mentioned before, we choose $N=6347$, and consider this as the eigenmode cutoff. This is because when $N=6347$, the factor of $\text{Exp} \left[-\frac{1}{2} k_{6347}^2 (r_i^2 + r_j^2) \right] \approx e^{-5} \approx 0.0067$ is very small. Therefore any eigenmodes with larger k_n^2 will contribute very little to the sum in Eq. (4.5), and can be neglected when calculating Ξ_{ij} .

On the other hand, if we want to implement RCM on Eq. (4.5), it is more useful to write the Ξ_{ij} matrix elements as:

$$\Xi_{ij} = -4 \sum_n \text{Exp} \left[-\frac{1}{2} k_n^2 (r_i^2 + r_j^2) \right] \cdot \frac{\phi_{n,i} \cdot \phi_{n,j}}{k^2 - k_n^2}, \quad (4.8)$$

where $\phi_{n,i}$ denotes the eigenfunction ϕ_n at port i .

The eigenfunctions ϕ_n in Eq.(4.8) are assumed to be Gaussian random variables.

And the PDF for eigenfunctions ϕ_n is:

$$P(\phi_n) = \frac{1}{\sqrt{2\pi\sigma^2}} \text{Exp} \left[-\frac{\phi_n^2}{2\sigma^2} \right], \quad \text{where } \sigma^2 = 1/A, \quad (4.9)$$

Therefore when implementing RCM, we actually generate eigenfunctions ϕ_n as random variables based on Eq. (4.9), instead of calculating them. However, we do not expect this assumption to be true for regular systems. We are just doing it for preliminary study purpose.

We generate the system's eigenvalues k_n^2 in Eq. (4.8) by calculating the eigenvalues of a $N \times N$ GOE random matrix and then apply a "mapping function", so that the GOE eigenvalues spectrum has uniform density as the rectangular box eigenvalues spectrum.

The raw GOE eigenvalue spectrum PDF obeys the "semi-circle" law:

$$P(\lambda_n) = \frac{2}{\pi\lambda_{n,max}} \sqrt{1 - \left(\frac{\lambda_n}{\lambda_{n,max}} \right)^2}, \quad \text{for } \lambda_n \in [-\lambda_{n,max}, \lambda_{n,max}], \quad (4.10)$$

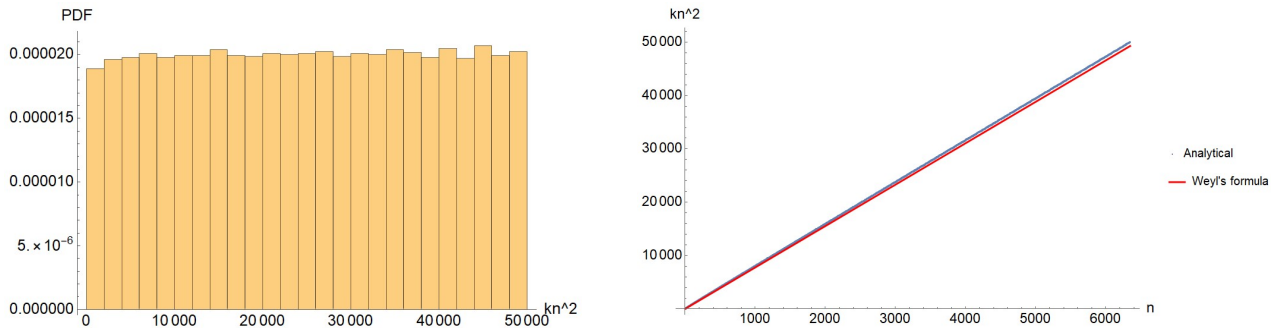
The mapping function we apply is:

$$M(\lambda_n) = \frac{4\pi}{A} \frac{N}{2\pi} \left[\pi + 2\sin^{-1}\left(\frac{\lambda_n}{\sqrt{2N}}\right) + 2\frac{\lambda_n}{\sqrt{2N}}\sqrt{1 - \frac{\lambda_n^2}{2N}} \right], \quad (4.11)$$

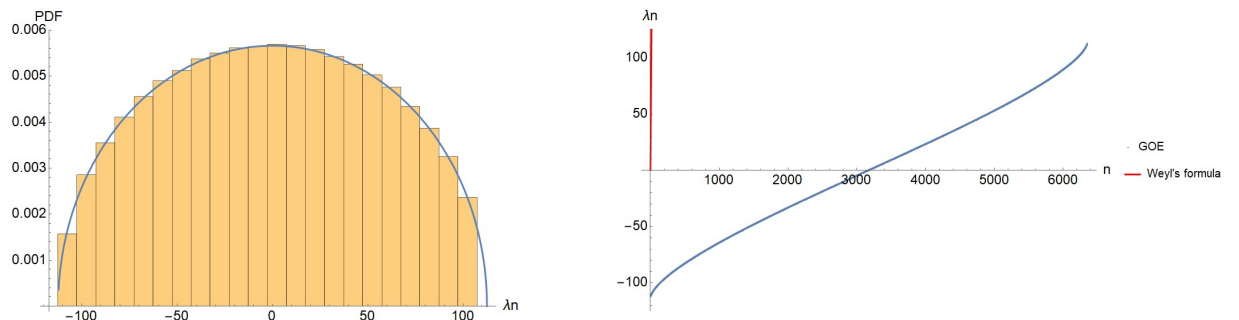
where $N = 6347$, λ_n are the eigenvalues of a $N \times N$ GOE matrix

This mapping function in Eq. (4.11) is intended to make the PDF of eigenvalues λ_n uniform in the range of: $0 < \lambda_n < k_N^2$.

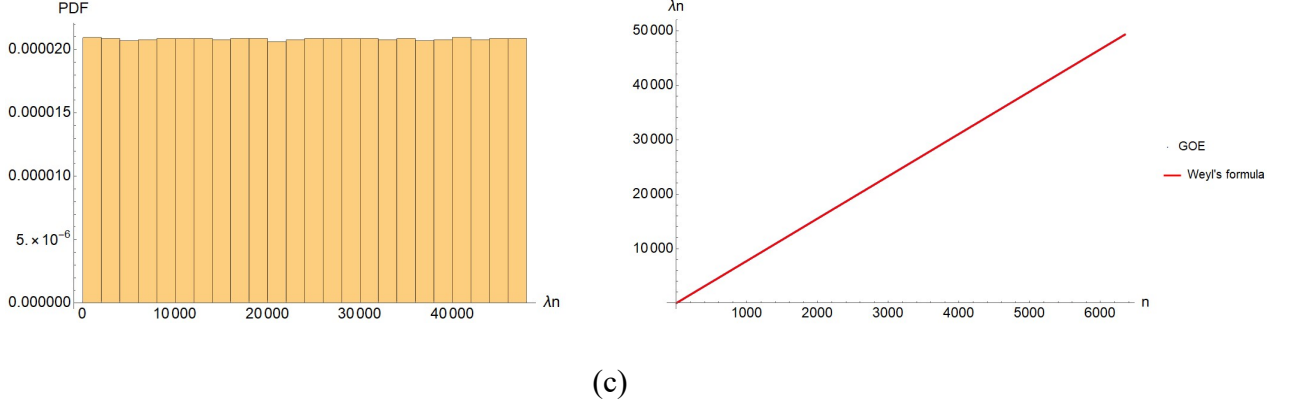
The mapped eigenvalue spectrum of the GOE random matrix will become uniform much alike the spectrum of the rectangular box, see Fig. 4.2. And the mapped GOE mean adjacent eigenvalue spacing $\Delta\lambda_n = \Delta(k_n^2) = 4\pi/A$. Once we map the GOE eigenvalue spectrum correctly, we can use the mapped eigenvalues λ_n to substitute for the rectangular box's eigenvalues k_n^2 .



(a)



(b)



(c)

Figure 4.2: (a) Rectangular box eigenvalue spectrum (left), and k_n^2 vs. n for rectangular box, analytical k_n^2 (blue dots) vs. Weyl's formula (red line) (right); (b) Raw 6347×6347 GOE random matrix eigenvalue spectrum (yellow histogram) vs. semi-circle law (blue line) (left), and λ_n vs. n for GOE eigenvalues, GOE eigenvalues (blue dots) vs. Weyl's formula (red line) (right); (c) Mapped 6347×6347 GOE random matrix eigenvalue spectrum (left), and λ_n vs. n for mapped GOE eigenvalues, mapped GOE eigenvalues (blue dots) vs. Weyl's formula (red line) (right).

4.2.2 Lossless Dimensionless Reactance PDF Using Numerical Eigenmodes vs.

Using the RCM

Given all the setup and the assumptions, now we can calculate the lossless dimensionless reactance PDF using the exact numerical eigenmodes (Eq. (4.7)) and using the RCM (Eq. (4.8)) proxy eigenfunctions and eigenvalues, and compare their results.

To make realizations of Eq. (4.7) and (4.8), the operating frequency ($k^2 = \omega^2/c^2$) has to be specified. We sample random values of k^2 assuming the PDF of k^2 is uniform within the operating frequency range. And we choose the operating frequency range of k^2 to be 8% of the range $[0, k_N^2]$, and symmetric about $\frac{1}{2} k_N^2$:

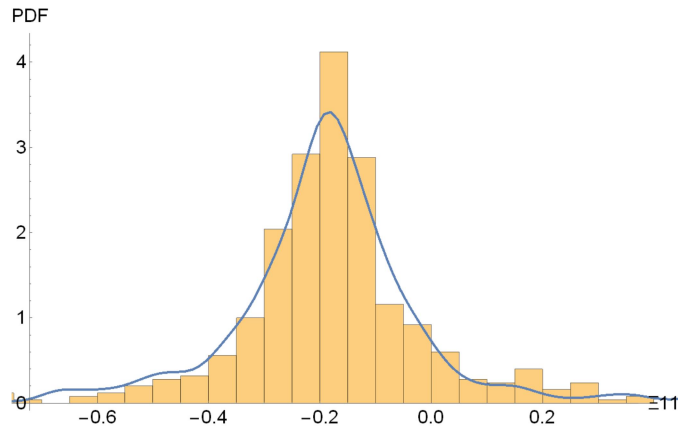
$$k^2 \in \left[\frac{1}{2}k_N^2 - 253\Delta(k^2), \frac{1}{2}k_N^2 + 253\Delta(k^2) \right] = [23032.6, 26976.1], \quad (4.12)$$

where $N = 6347, \Delta(k^2) = 4\pi/A \approx 7.77$,

For each time of the realization, we need to randomly generate a new value for k^2 .

We choose a rather narrow operating frequency range of k^2 , because we want to keep the radiation resistance to be roughly a constant over the range of the calculation. Since the operating frequency range contains roughly 500 eigenmodes, to avoid oversampling or undersampling, we choose the number of realizations to be 500.

The results of the dimensionless reactance PDF using the exact eigenvalues and eigenfunctions vs. the RCM prediction are plotted in Fig. 4.3. In our two-port rectangular box case, the dimensionless reactance Ξ is a 2×2 matrix. And Ξ_{11} has the same PDF as Ξ_{22} , while Ξ_{12} has the same PDF as Ξ_{21} . Therefore, I only need to plot for the PDF of Ξ_{11} and Ξ_{12} .



(a)

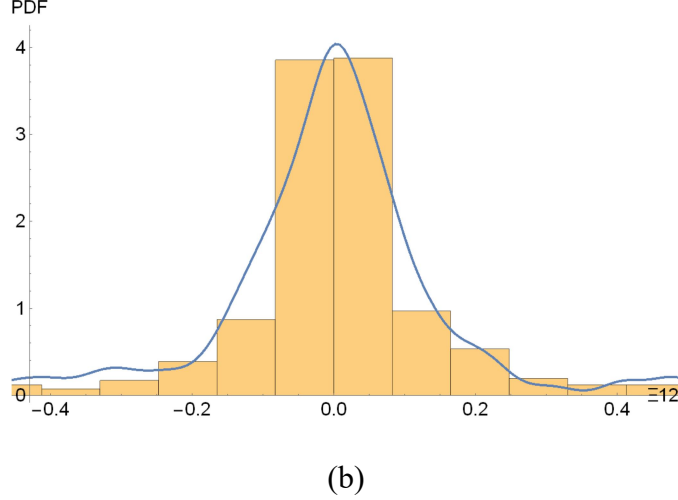


Figure 4.3: Lossless dimensionless reactance PDF, 500 realizations, GOE has 50 Gaussian orthogonal random matrices. (a) Ξ_{11} using the exact eigenvalues and eigenfunctions (yellow histogram) and using the RCM (blue line), (b) Ξ_{12} using the exact eigenvalues and eigenfunctions (yellow histogram) and using the RCM (blue line).

Fig. 4.3 shows that the lossless dimensionless reactance PDF using the exact eigenvalues and eigenfunctions and using the RCM don't have good agreement. Nor do we expect them to have good agreement, because we make this preliminary study based on a false assumption that the rectangular box is a chaotic system.

4.3 Impedance for Lossy Two-Port 2D Rectangular Cavity

4.3.1 Formulas for Lossy Impedance

For a lossy cavity with M ports, the impedance matrix \mathbf{Z} is given by [1, 6]:

$$Z_{ij} = -jkh\eta_0 \sum_{n=1}^N \frac{\langle u_i \phi_n \rangle \langle u_j \phi_n \rangle}{(1 - jQ^{-1})k^2 - k_n^2}, \quad (4.13)$$

The lossy impedance formula (Eq. (4.13)) is the same as the lossless impedance formula (Eq. (4.3)), except for the $(1 - jQ^{-1})$ term in the denominator. The quantity Q is the quality factor of the cavity, higher Q value means lower loss. When $Q \rightarrow +\infty$, the lossy impedance formula becomes the lossless formula. The physical meaning of all the other quantities is the same as in Eq. (4.3).

Likewise, we can define the lossy dimensionless impedance matrix as:

$$\boldsymbol{\zeta} = -\frac{j}{\pi} \sum_n \frac{\mathbf{w}_n \mathbf{w}_n^T}{(1 - jQ^{-1})\tilde{k}^2 - \tilde{k}_n^2} \quad (4.14)$$

so that:

$$\mathbf{Z} = \frac{kh\eta_0}{4} \boldsymbol{\zeta}, \quad (4.15)$$

where all the definitions of \mathbf{w}_n , \tilde{k}^2 and \tilde{k}_n^2 are the same as in lossless case.

When using numerical eigenmodes to evaluate the dimensionless impedance, it's more convenient to express $\boldsymbol{\zeta}$ as:

$$\begin{aligned} \zeta_{ij} = \frac{16i}{A} \sum_{n=1}^N \text{Exp} \left[-\frac{1}{2} k_n^2 (r_i^2 + r_j^2) \right] \cdot \sin \left(\frac{n_x \pi}{a} x_i \right) \sin \left(\frac{n_y \pi}{b} y_i \right) \\ \cdot \sin \left(\frac{n_x \pi}{a} x_j \right) \sin \left(\frac{n_y \pi}{b} y_j \right) / [(1 + iQ^{-1})k^2 - k_n^2], \end{aligned} \quad (4.16)$$

While when implementing the RCM to calculate the dimensionless impedance, it's more convenient to express $\boldsymbol{\zeta}$ as:

$$\zeta_{ij} = 4i \sum_n \text{Exp} \left[-\frac{1}{2} k_n^2 (r_i^2 + r_j^2) \right] \frac{\phi_{n,i} \cdot \phi_{n,j}}{(1 + iQ^{-1})k^2 - k_n^2} \quad (4.17)$$

All the other numerical setup are the same as in lossless case, such as the cutoff $N=6347$, the mapping function, the PDF for ϕ_n and so on.

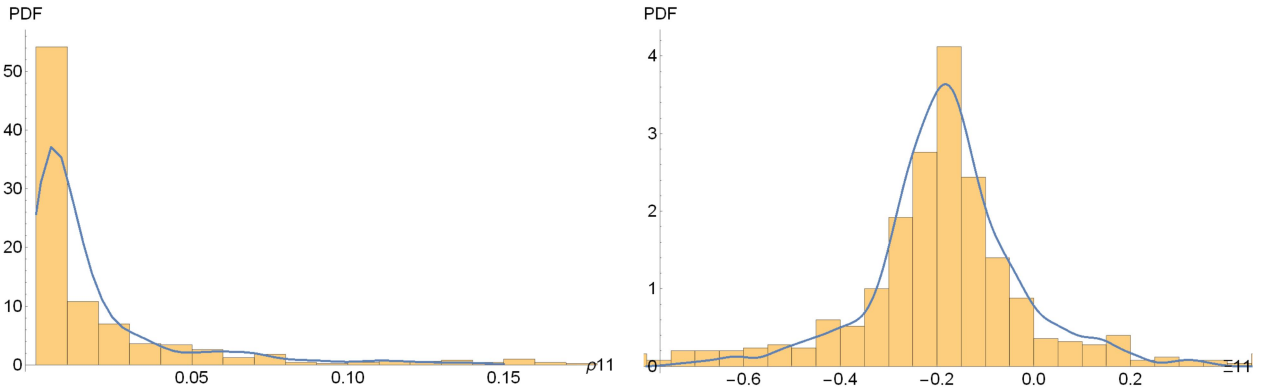
Obviously, in a lossy cavity case, the impedance has both a real part and an imaginary part. And by definition:

$$\zeta = \rho + j\Xi = \text{Re}[\zeta] + i\text{Im}[\zeta],$$

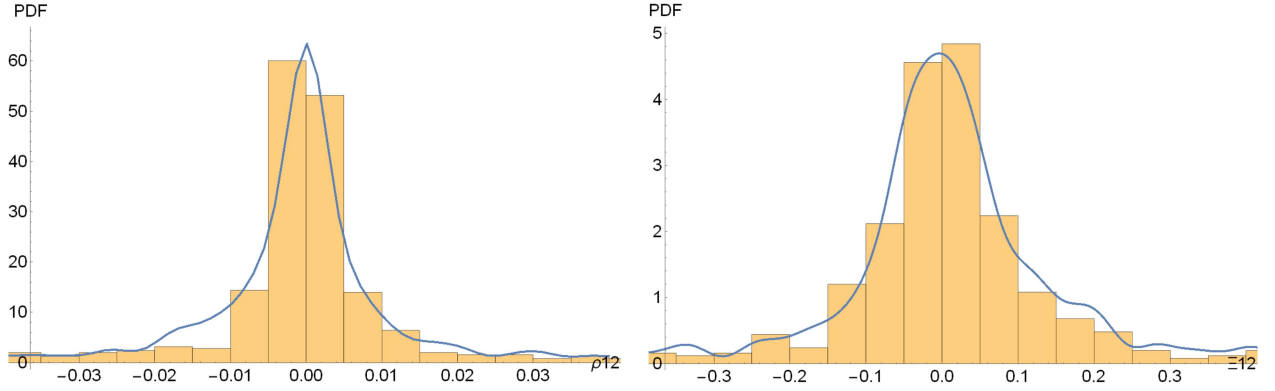
$$\text{where } \begin{cases} \rho = \text{Re}[\zeta], & \text{is the dimensionless resistance matrix} \\ \Xi = -\text{Im}[\zeta], & \text{is the dimensionless reactance matrix} \end{cases} \quad (4.18)$$

4.3.2 Lossy Dimensionless Impedance PDF Using Numerical Eigenmodes vs. Using the RCM

The assumptions and the method we employ to calculate the lossy dimensionless impedance are the same as those we use to calculate the lossless dimensionless reactance, see section 4.2.2 for details. In the lossy case the equations we are use are different (Eq. (4.16) for numerical eigenmodes simulation and Eq. (4.17) for the RCM). Here I only list the final results for a two-port lossy dimensionless impedance PDF.



(a)



(b)

Figure 4.4: Low loss dimensionless impedance PDF, quality factor $Q = 10^5$ (loss parameter $\alpha = k^2/(\Delta(k^2)Q) \approx 0.032$), 500 realizations, GOE has 50 Gaussian orthogonal random matrices, ρ ($\text{Re}[\zeta]$) on the left and Ξ ($-\text{Im}[\zeta]$) on the right. (a) ζ_{11} using numerical eigenmodes (yellow histogram) and using the RCM (blue line), (b) ζ_{12} using numerical eigenmodes (yellow histogram) and using the RCM (blue line).

First let's look at a rather low loss cavity case, when the cavity quality factor $Q = 10^5$ (loss parameter $\alpha = k^2/(\Delta(k^2)Q) \approx 0.032$), the low loss dimensionless impedance PDF results are plotted in Fig. 4.4. From these results, we can see that: (1) since the cavity quality factor $Q = 10^5$ is rather high, the dimensionless resistance ρ is usually much smaller than the dimensionless reactance Ξ in terms of magnitude, (2) the low loss dimensionless reactance Ξ has a rather similar PDF compared with lossless case, see Fig. 4.3, (3) comparing with the lossless case, the low loss dimensionless reactance PDF using the RCM has a little better agreement with the PDF using the exact eigenmodes.

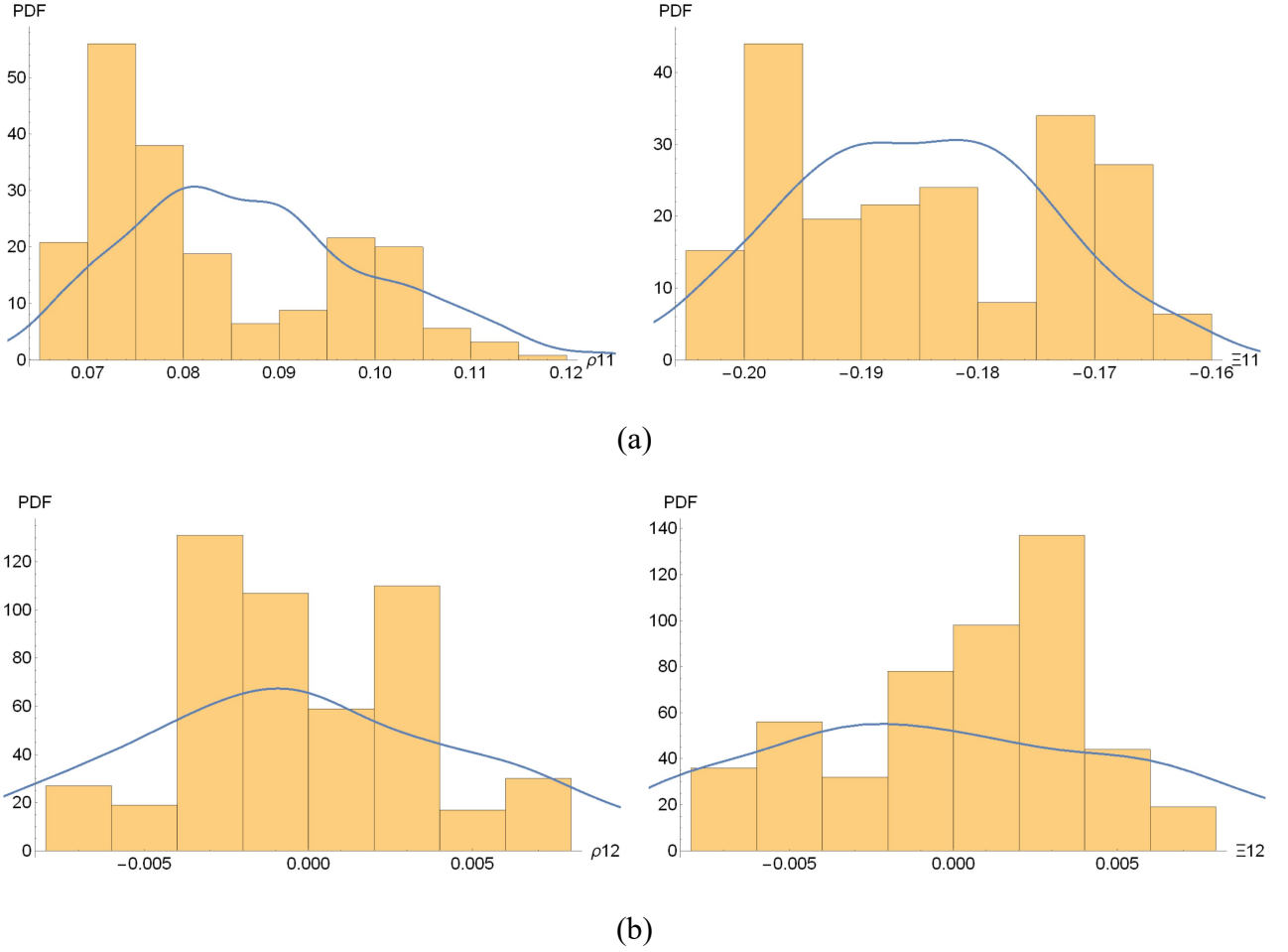


Figure 4.5: High loss dimensionless impedance PDF, quality factor $Q = 100$ (loss parameter $\alpha = k^2/(\Delta(k^2)Q) \approx 32.20$), 500 realizations, GOE has 50 Gaussian orthogonal random matrices, $\rho(\text{Re}[\zeta])$ on the left and $\Xi(-\text{Im}[\zeta])$ on the right. (a) ζ_{11} using numerical eigenmodes (yellow histogram) and using the RCM (blue line), (b) ζ_{12} using numerical eigenmodes (yellow histogram) and using the RCM (blue line).

Second we turn to look at a high loss cavity case, when the cavity quality factor $Q = 100$ (loss parameter $\alpha = k^2/(\Delta(k^2)Q) \approx 32.20$), the high loss dimensionless impedance PDF results are plotted in Fig. 4.5. From these results, we can see that: (1) in the high loss case, the dimensionless resistance ρ is usually comparable to the

dimensionless reactance Ξ in terms of magnitude, (2) the high loss dimensionless impedance ζ has a totally different PDF than lossless or low loss cases, (3) the high loss dimensionless impedance PDF using the RCM is very different from the PDF using the exact eigenmodes. And since loss parameter α is too high, there is no statistical pattern in the high loss dimensionless impedance PDF at all.

Chapter 5: Summary and Future Work

5.1 Summary

In summary, my study of mixed wave systems includes these three parts:

1. Study of billiard systems with the “Four Arcs” and the “Peanut” boundary shape. The billiard trajectories in real space and in phase space together show that regular and chaotic trajectories coexist in these two systems. Both Four Arcs and Peanut systems have been verified to be mixed systems.
2. Implementation of the Method of Moments (MOM) to solve the eigenfrequencies and eigenmodes of a circular cavity for preliminary testing purpose. Furthermore I solve the eigenfrequencies and eigenmodes of mixed systems: the Four Arcs and the Peanut cavities. The numerical eigenfrequencies and eigenmodes are necessary information for the generalized Random Coupling Model (RCM) on mixed systems.
3. Preliminary study of the lossless and lossy impedance of a 2D two-port rectangular cavity, with Gaussian profile port function. The RCM is applied to this 2D rectangular cavity as if it were a chaotic system. The lossless and lossy impedance PDF using exact eigenmodes and using the RCM were compared.

5.2 Future Work

These tasks are left for future work:

1. Given the Four Arcs and Peanut billiard trajectories in real space and in phase space, we have found that these two mixed systems have multiple intermixed chaotic/regular regions, which makes these two mixed systems more generic and complicated than the “Mushroom” mixed system studied before [3]. How to separate the regular and chaotic regions for these two more generic mixed systems is a problem left for future study.
2. Although MOM can solve for the eigenfrequencies and eigenmodes of our concerned 2D cavities, I also find that it will miss finding some eigenmodes of a regular system (or miss finding some regular eigenmodes of a mixed system). For a circular cavity, my MOM numerical solver will miss finding roughly 3% of the total eigenmodes. Next we need to figure out some method to either find all these regular eigenmodes precisely or to prove that missing a small portion of regular eigenmodes won't matter the mixed system cavities' impedance statistics.
3. I only apply the RCM to one regular system: 2D rectangular cavity. Therefore future work needs to really generalize the RCM to mixed systems and study Four Arcs and Peanut cavity impedance in a statistical point of view.

Bibliography

- [1] Xing Zheng, “Statistics of Impedance and Scattering Matrices in Chaotic Microwave Cavities: the Random Coupling Model”, Ph.D. thesis, University of Maryland, 2005.
- [2] Ming-Jer Lee, “Statistical Modeling of Wave Chaotic Transport and Tunneling”, Ph.D. thesis, University of Maryland, 2013.
- [3] Ming-Jer Lee, Thomas Antonsen, and Edward Ott, “Statistical model of short wavelength transport through cavities with coexisting chaotic and regular ray trajectories”, *Phys. Rev. E*, vol. 87, 062906, 2013.
- [4] Edward Ott, *Chaos in Dynamical Systems, 2nd Edition*, Cambridge University Press, Cambridge, England, 2002.
- [5] Sameer Hemmady, Thomas Antonsen, Edward Ott, and Steven Anlage, “Statistical Prediction and Measurement of Induced Voltages on Components Within Complicated Enclosures: A Wave-Chaotic Approach”, *IEEE Transactions on Electromagnetic Compatibility*, vol. 54, No. 4, August 2012.
- [6] Gabriele Gradoni, Jen-Hao Yeh, Bo Xiao, Thomas Antonsen, Steven Anlage, and Edward Ott, “Predicting the statistics of wave transport through chaotic cavities by the random coupling model: A review and recent progress”, *Wave Motion* 51, 606-621, 2014.
- [7] Jian-Ming Jin, *Theory and Computation of Electromagnetic Fields, 2nd Edition*, IEEE Press, John Wiley & Sons, Hoboken, New Jersey, 2015.

- [8] Thomas Rylander, Par Ingelstrom, and Anders Bondeson, *Computational Electromagnetics, 2nd Edition*, Springer, New York, 2013.
- [9] Walton Gibson, *The Method of Moments in Electromagnetics, 2nd Edition*, CRC Press, New York, 2015.
- [10] Steven McDonald and Allan Kaufman, “Wave chaos in the stadium: Statistical properties of short-wave solutions of the Helmholtz equation”, *Phys. Rev. A*, vol. 37, 3067, April 15, 1988.
- [11] R. J. Riddell, “Boundary-Distribution Solution of the Helmholtz Equation for a Region with Corners”, *Journal of Computational Physics*, 31, 21-41, 1979.